SIMULATION OF GLASS MELTER PERFORMANCE

by

Kwang J. Won

B. S., Seoul National University
(1966)

Submitted in Partial Fulfillment

of the Requirements for the

Degree of Master of Science

at the

MASSACHUSETTS INSTITUTE OF TECHNOLOGY

January 23, 1974

Signature of Author: _____
Department of Chemical Engineering
January 23, 1974

Certified by : _____
Thesis Supervisor

Certified by: _____
Thesis Supervisor

Accepted by: _____
Chairman, Dept. Comm. on Graduate
Theses

ABSTRACT

SIMULATION OF GLASS MELTER PERFORMANCE

by

Kwang J. Won

Submitted to the Department of Chemical Engineering in February 1974, in partial fulfillment of the requirements for the degree of Master of Science in Chemical Engineering.

The three dimensional natural convection flow and temperature distributions in glass furnace were obtained through the use of source-sink approximation method. In this method, assumption was made that three dimensional flow and temperature distributions may be represented by the sum of the flow and temperature distributions in two orthogonal planes. These orthogonal planes are linked by distributed sources and sinks of energy. Thus by obtaining a series of two dimensional solutions, a composite of three dimensional approximation solution may be obtained.

Thesis Supervisor: Adel F. Sarofim
Professor of Chemical Engineering

Thesis Supervisor: Lloyd A. Clomburg
Assistant Professor of Chemical Engineering

Department of Chemical Engineering
Massachusetts Institute of Technology
Cambridge, Massachusetts 02139

January 23, 1974

Professor David B. Ralston
Secretary of the Faculty
Massachusetts Institute of Technology
Cambridge, Massachusetts 02139

Dear Professor Ralston:

In accordance with the regulations of the Faculty, I herewith submit a thesis, entitled "Simulation of Glass Melter Performance", in partial fulfillment of the requirements for the degree of Master of Science in Chemical Engineering at the Massachusetts Institute of Technology.

Respectfully submitted,

Kwang J. Won

ACKNOWLEDGEMENT

The subject of this work was suggested to the author by his thesis supervisor, Professor A. F. Sarofim. His guidance throughout this work is gratefully acknowledged. In addition, the author would like to thank Professor L. A. Clomburg and Mr. N. W. E. Curlet for their helpful suggestions.

The work was typed by Mrs. E. D. Kehoe. Her efforts are greatly appreciated.

TABLE OF CONTENTS

TABLE OF CONTENTS (Continued)

LIST OF FIGURES

LIST OF FIGURES (Continued)

LIST OF TABLES

I. SUMMARY

In this thesis, three-dimensional natural convection in glass melts is studied by means of an approximate numerical technique, referred to as the source-sink approximation method. In this method, the transport in the third dimension is modeled as a two-dimensional natural convection problem with sources and sinks of energy distributed throughout the plane of motion.

The previous work performed in this department by Noble (12) and Clomburg (4) was concerned with the two-dimensional problem. However, the three-dimensional problem is the more descriptive of the actual flow phenomena. For three-dimensional natural convection problems, classical solution techniques are not, in general, feasible and since exact solutions are certainly not attainable, one must resort to some approximation method. A few authors (1, 3, 19) have suggested numerical methods for primitive three-dimensional equations. Their application on the prototype furnace will undoubtedly accompany operation difficulties associated with numerical instability and intolerable computation storage requirements and machine time. The principle difficulties arise because interesting problems are described by large Rayleigh numbers (ca. 10^7-10^8) and thus require detailed meshes to obtain resolution of the boundary layer

type flows that develop. Even with today's fast digital computers, the task is prohibitively expensive, if at all possible (2).

Quite often some knowledge can be obtained by solving a number of more tractable equivalent two-dimensional problems. The major aim of this thesis is to develop and text a simple technique for selecting those two-dimensional problems. This purpose has been achieved through the introduction of a source-sink approximation method. The source-sink functions were obtained from the known approximate solution of the two dimensional flow and energy equation for the orthogonal plane. For the transverse section, for example, these functions can be written in the form of

$$SI_T = - \left.\frac{\partial^2 \theta}{\partial x^2}\right|_L - \Phi_L \qquad (1)$$

where θ and Φ_L represent the temperature distribution and the source-sink function in the longitudinal section, respectively.

With this function, the following coupled flow and energy equations are numerically solved via finite-difference method.

Energy Equation

$$\frac{\partial \theta'}{\partial t} + \frac{\partial u\theta'}{\partial x} + \frac{\partial w\theta'}{\partial z} = \frac{\partial^2 \theta'}{\partial x^2} + \frac{\partial^2 \theta'}{\partial z^2} + SI_T \qquad (2)$$

where θ' represents the temperature distribution in a transverse section.

Flow Equation

$$\frac{1}{N_{Pr}} \frac{\partial \nabla^2 \psi}{\partial t} + \frac{\partial}{\partial x} (u \nabla^2 \psi) + \frac{\partial}{\partial z} (w \nabla^2 \psi) =$$

$$- N_{RA} \frac{\partial T}{\partial z} + \frac{\partial}{\partial x} (\nu \frac{\partial \nabla^2 \psi}{\partial x}) + \frac{\partial}{\partial z} (\nu \frac{\partial \nabla^2 \psi}{\partial z}) \qquad (3)$$

The hydrodynamic and thermal boundary conditions are of course specified.

The basic method of solution involves casting the problem as a transient initial value problem and extending the solution to steady-state. For this purpose, both motionless isothermal initial conditions or the results of a previous run were used to start the calculations. Since the basic equations are identical with the Clomburg problem (4), his computer program, CONRAD, was used with slight change. Therefore, his work serves as a starting point of this investigation.

The proposed method was applied to the real green glass furnace. Effort has been made to retain the salient feature of the prototype as far as possible. The results obtained have shown characteristics of three-dimensional flow patterns, thus appearing as feasible. One of the most prominent features is the formation of four circulation cells under the batch cover. However in the light of the imposed assumptions and approximations, these results should be checked by more rigorous solutions and by experimental data.

Finally, some mention should be made about the computation time. A typical run with a 15x16 zone arrangement only required 0.0022 CPU minute/iteration on an IBM Model 370/165. For the maximum number of zones (20x40), the CONRAD 8 program uses less than 1 minute of CPU minutes for 200 iterations on this machine. With proper choice of time step parameters, convergence of the computations is normally achieved after 100-150 iterations.

II. INTRODUCTION

A. Glass Furnace

A glass furnace is a large tank made of refractory in which the necessary heat is provided by gas or oil flames through the combustion ports. A detailed qualitative description of a glass furnace and its operation can be found elsewhere (8).

One type of furnace for which this thesis is relevant is the large continuous tanks used in the production of container, bottle, and plate, of which the dimensions may be 20-100 feet long, 10-30 feet wide and 2-4 feet deep. The furnaces may contain up to 50-200 tons of molten glass and have throughput as large as 10-60 tons/day.

One of the most common forms of construction is the cross-fired throat tank, as shown in Figure 1. The furnace consists of two chambers separated by a refractory wall through which there is a channel, the throat. In the larger melting chamber, the raw materials are melted and reacted and the glass produced is refined. In the working chamber, the glass cools and is further refined prior to being fed to the forming machines. The homogenization of glass melts is mainly achieved in the melting chamber.

The surface of the glass melt in the melting chamber shows three distinct regions. A definite portion of the glass furnace is always covered with batch heap (unreacted

Fig. 1 CROSS FIRED GLASS FURNACE

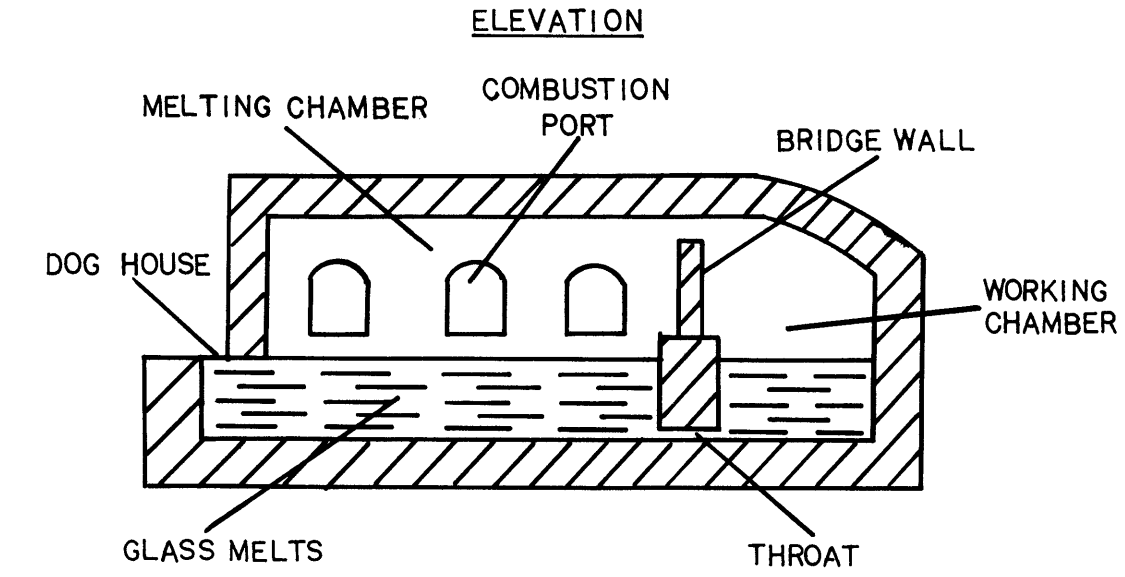

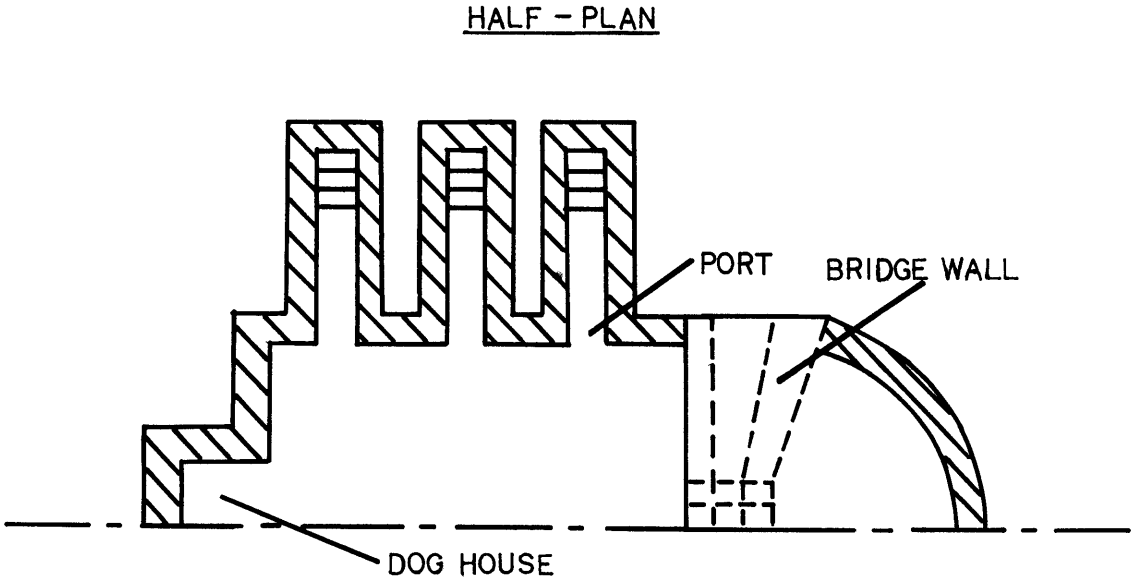

raw materials). An adjoining surface zone has a layer of foam and froth, while the remaining large portion of area is relatively flat and clear.

The raw materials - a mixture in precise proportions of sand, soda ash, and limestone with various additives - are added continuously at the doghouse, thus forming batch heap. They are melted by the heat supplied by flames in combustion space. The melting process involves chemical reactions, the generation of gaseous products, the formation of silicates and the mixing of the liquid components. The gaseous products, mainly CO_2, SO_2 and H_2O, partly escape into the combustion space and partly remain in the molten glass.

Disengagement of these gases from the melt constitutes the second part of the process taking place in the furnace, namely, refining. During refining, the rising of the disentrained gas bubbles stirs the melt and improves its homogeneity. The thorough mixing of the entire melt, however, is solely achieved by natural convection, which results from local temperature differences in the melting chamber. The temperatures in the melting chamber range from 2400°F to 2900°F in the glass melt and about 3100°F in the combustion space.

The circulatory flows and mixing in the glass tank are mainly engendered by the addition of energy to the top surface of the melt and the removal of energy along the

batch cover, walls and bottom of the furnace. Computed results and experimental study (4) indicate that the melt is thermally stratified in the bulk of the enclosure. Regions of large temperature gradient exist only under the top surface and along the end walls. There temperature gradients act in the nature of a "thermal pump" and produce the basic fluid motion which consists of two large circulation cells. The flow pattern for the longitudinal cross-section is shown in Figure 2. The largest circulation cell, centered near the upper left corner, extends almost completely across the enclosure, and serves to transport most of the energy from the source to the batch cover and left-hand sinks (doghouse wall). Material is accelerated as it picks up energy from the source, and then is decelerated as it is cooled under the top sink and along the left side wall. When the material encounters its "own" temperature level, it leaves the boundary layer to enter the core. The smaller cell is relatively weak and is driven by the primary cell and right wall heat losses. The flow pattern for a transverse cross-section is shown in Figure 3. Unfortunately, the investigated regions have been limited to a cross-section made somewhere in the open area of a furnace, that is, not under the batch. Therefore, the results of Trier (19) and Clomburg (4) appear qualitative. From their results, the circulation rates in transverse section are weaker than in longitudinal section. Hot melt flows down the cooler side walls to the

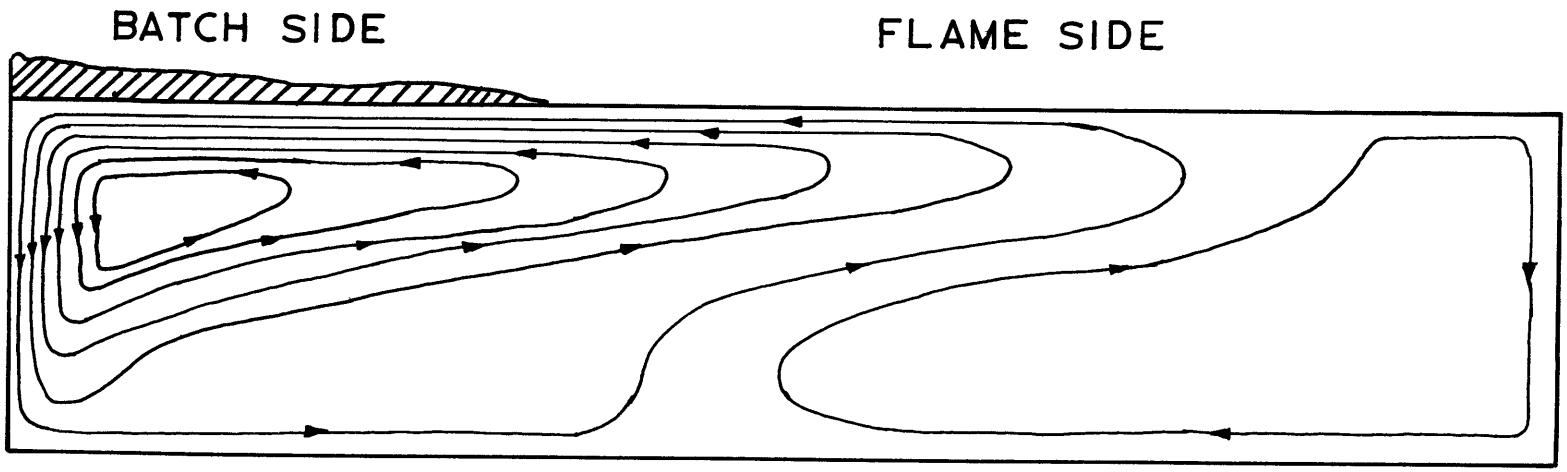

Figure 2. Flow Pattern in Longitudinal Section of a Glass Furnace

Figure 3. Flow Pattern in Transverse Section of a Glass Furnace

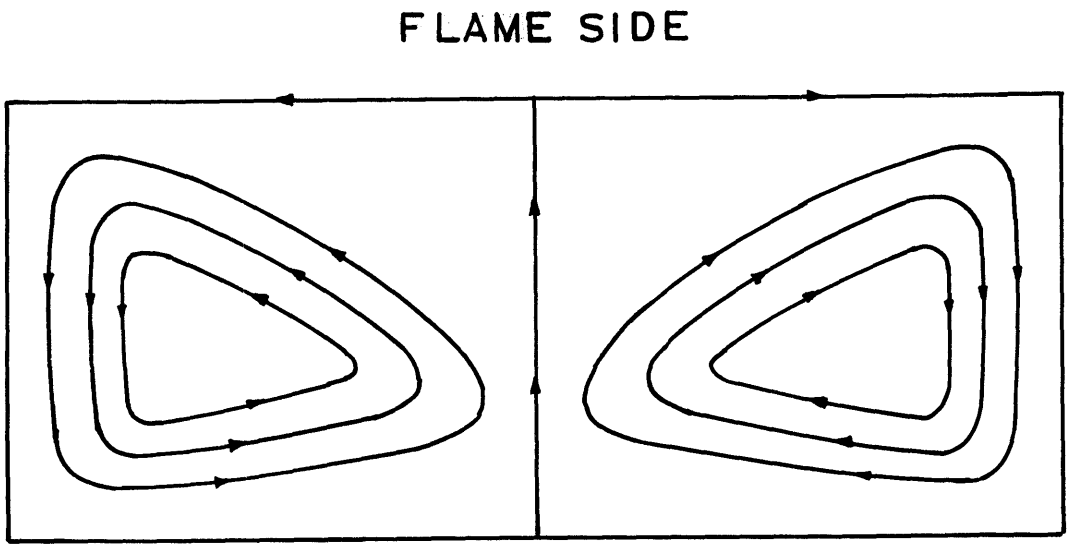

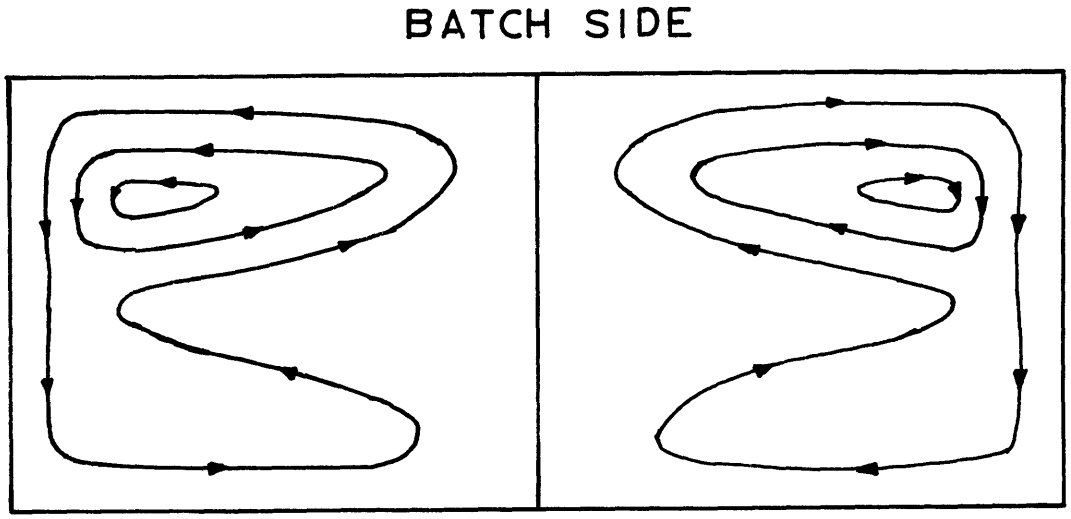

bottom, and then up in the middle of the tank. These cells also mix the melt and transfer energy to the cooler sections of the furnace.

This thesis provides a quantitative description of the transverse section flows under the batch cover. As will be shown later, the flow patterns in this region are quite different from the above description.

The design and operation of glass melting furnaces have evolved as an empirical art since glass making began. However, it has been recognized that the natural convection within the melt homogenizes the glass and that the modification of these currents can exert a profound influence on product quality. The study of natural convection in a fluid should yield results which would be useful in predicting the performance of glass furnace particularly with regard to the circulation currents.

B. Previous Work

The work reported here is a part of a continuing program for the investigation of radiation and natural convection interaction performed in this department. The previous works by Noble (12) and Clomburg (4), representing the most significant work in this program, were concerned with the two-dimensional problem only. Clomburg's results are the most relevant to this work and serves as a starting point to this thesis.

Clomburg obtained a highly generalized two-dimensional mathematical model of a glass furnace by making allowance for buoyancy, temperature-dependent viscosity and diffusive radiation. To solve the time-dependent, coupled flow and energy equation, the computer program, CONRAD, was written. With the aid of this program, he obtained numerical solutions up to Rayleigh number $\sim 10^8$ and performed an experimental work with a simple model of a glass tank to verify the numerical results. His results are largely concerned with the longitudinal section flow patterns.

Trier (19) has presented the stream function and temperature fields for a transverse section of a glass tank. His results were obtained by the numerical solution of the biharmonic equation and the energy equation by a relaxation procedure developed by Peschke (15). The boundary conditions were: specified temperatures along all surfaces and a shear free top surface. (Only the half section of the transverse plane was considered due to its symmetry.) Trier considered both constant and temperature dependent viscosity and thermal conductivities to obtain solutions for Rayleigh numbers of $\sim 10^6$. The results are similar to those obtained by Clomburg (4).

The three-dimensional solution of the natural convection equations has received little attention because of the complexity, but they have been investigated by a few authors.

Aziz and Hellums (1) studied the natural convection problem in a cube of specified temperatures on the upper and lower walls (heat from below) with insulated side walls. They succeeded in obtaining a solution of the equations of motion and energy in three dimensions by numerical finite difference method.

The complete Navier-Stokes equations were cast in terms of three-dimensional vorticity and a vector potential. The resulting equations were solved using an alternating direction method for the parabolic portion of the problem, and Succusive Over-Relaxation for the elliptic portion. It was also shown that the proper boundary condition on the normal component of velocity (no slip condition) is satisfied if the normal derivative of the normal component of the vector potential vanishes, and if the components of the vector potential tangential to the surface vanishes. For a fluid with constant properties and Pr=1, they obtained a solution for Ra=3500.

Chorin (3) has solved the primitive flow equations by decomposing the Navier-Stokes Equation into two functions, one for the velocity and the other for pressure. The velocity at the new iteration is approximated by an implicit solution of the flow equation without the pressure term. Then the velocity and pressure are calculated by the iterative solution of the continuity equation and an equation

for the velocity with the pressure term. He solved the three dimensional natural convection problem of a fluid heated from below (Bernard Convection Cell problem) for Rayleigh Numbers of 10^3.

William (21) solved the problem of natural convection of an incompressible fluid in a vertical rotating annulus with walls at different temperature. He used an explicit scheme for the primitive velocity and energy equations; the pressure was obtained by the solution of Poisson's equation using trigonometric interpolation procedures.

These methods have only been tested for low Rayleigh numbers, $\sim 10^3$, and their extension to higher values, $\sim 10^7$, is questionable.

Most recently, Chen and Goodsen (2) adapted the numerical algorithm by Aziz and Hellums to the application on an electrical glass furnace. The temperature and velocity profiles generated appeared reasonable. The computer time required to obtain a solution was reported about 70 minutes on CDC 6500 with uniform grid 11x11x11. This coarse grid system is in contrast to the refined grid found necessary by Clomburg to achieve realistic results.

In the numerical studies of fluid dynamics problems there generally exists regions of maximum change in flow profiles. It has been implicitly assumed that the use of nonuniform grids, with greatest resolution in the expected

region of maximum change, produces minimum overall errors in finite-difference solutions of a system of two non-linear coupled higher order differential equations. However, some reports (4, 20) have indicated that unless precautions are taken to select a prudent grid arrangement, a coarse grid system can introduce quite spurious effects on the overall results. Recently, Crowder and Dalton (5) examined this assumption. They found that the use of grids with discontinuously varying spacing gave poorer results than those obtained with regular uniform grids with the same number of points. However, it is clearly undesirable to use more grid points than required to resolve the boundary layer, because finer uniform meshes always make the total computation time prohibitively large. An obvious remedy was found by Rivas (16). It was shown that stretched coordinates could be used to obtain a nonuniform grid system which reduced the truncation error introduced by irregular nonuniform grids. The optimum number of intervals to resolve a boundary layer adequately was reported to be at least three (11, 17).

Relevant experimental work is under way in this department by N.W.E. Curlet. He will obtain experimental data for the three dimensional temperature and flow patterns in a simplified glycerin model of glass furnace.

III. DEVELOPMENT OF EQUATIONS

For three-dimensional natural convection problems, classical solution techniques are not, in general, feasible and since exact analytical solutions are certainly not attainable, one must resort to some approximation method. Quite often some knowledge of the three-dimensional temperature and flow distribution can be obtained by solving the more tractable equivalent two-dimensional problems. The present approach utilizes a technique matching two orthogonal solutions of two-dimensional problems, in order to make the composite represent a good approximation to a three-dimensional natural convection problem.

A. Statement of Problem

Since this is one of the first attempts at a three-dimensional problem, all the complexities of the glass furnace were not attempted. Instead, only the convective profiles generated in the furnace are considered. As already mentioned, the homogenization of glass melts are mainly achieved in the melting chamber. It is also believed that only a small portion of the melting chamber near the inlet surface is used for a reaction and melting. Therefore, the present problem attempts to simulate the convective flow profiles in a melting chamber without consideration of the reaction and melting processes. For further simplification,

no material throughput is allowed and all physical properties are assumed constant except viscosity and density. (However, effects of radiant heat transfer is incorporated using an effective thermal conductivity according to the Rosseland diffusion approximation for an optically thick fluid (4).)

The geometry and boundary conditions of the problem are summarized in Figure 4. Cartesian coordinates (x,y,z) have been introduced with origin at the front left corner apex of the rectangular bath glass furnace, which has the dimension of height H, length L and width W. The gravity acts in the x-direction.

The batch cover is idealized as a plane of extent, B, which is maintained at some appropriate sink temperature T_S, representative of the bottom surface temperature of the batch. For the simplicity of the calculation, it is assumed that heat transfer into the melt by flame radiation is idealized by some assumed energy flux, q_F, and the end walls, the side walls and the bottom of the furnace lose heat to the ambient at temperature T_A and that these walls and bottom have appropriate overall heat transfer coefficients U.

B. Derivation of General Governing Equations

For a variable viscosity, incompressible flow, the transient governing differential equations describing the behavior of a fluid for three dimensional natural convection are given by the usual Boussinesq Approximation as:

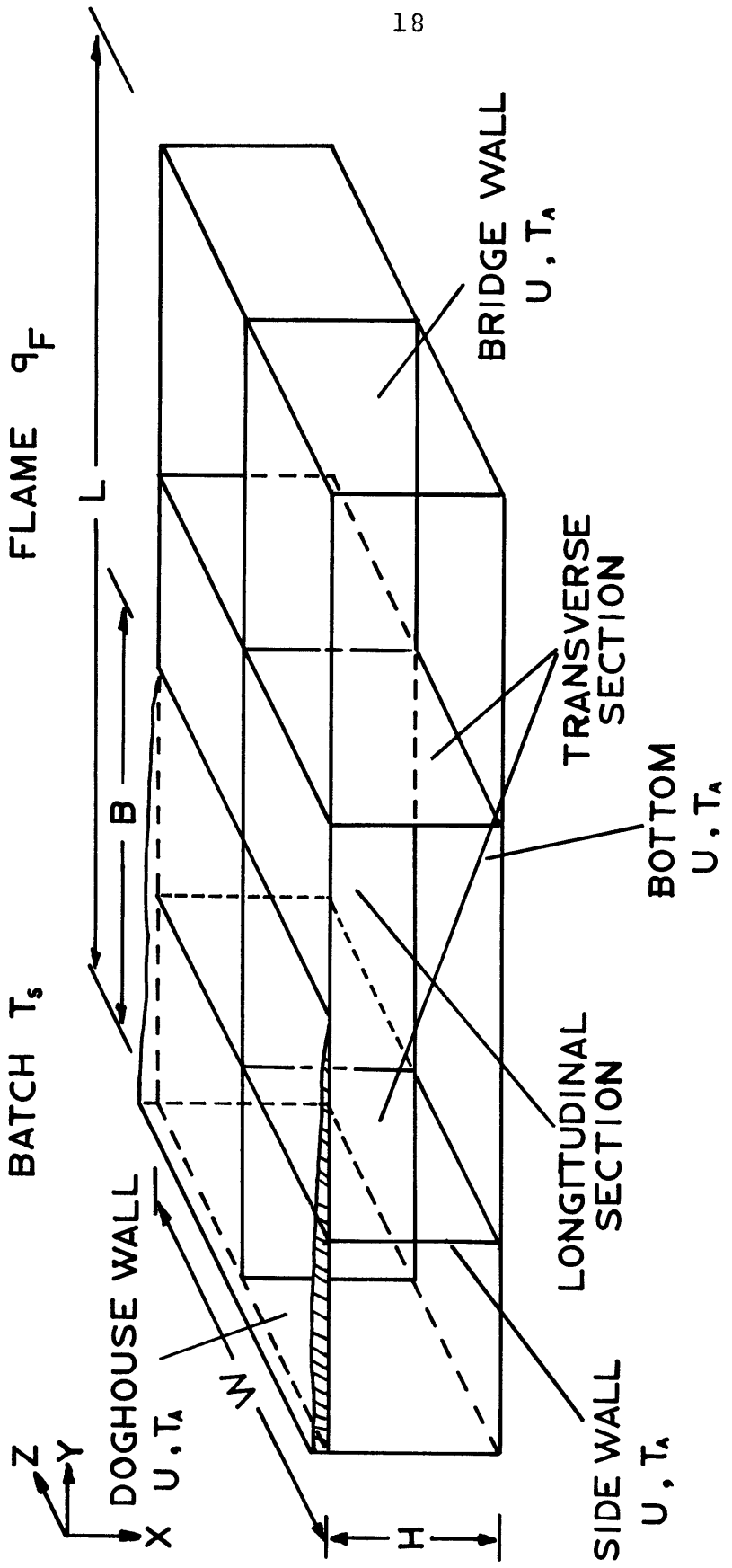

Figure 4. Schematic Diagram of Glass Furnace for Mathematical Modeling

Momentum Equation

$$\frac{Du}{Dt} = g\beta(T-T_o) - \frac{1}{\rho_o}\frac{\partial P}{\partial x} + \frac{1}{\rho_o}[\nabla\cdot\mu\nabla u + \frac{\partial \vec{v}}{\partial x}\cdot\nabla\mu] \quad (1)$$

$$\frac{Dv}{Dt} = - \frac{1}{\rho_o}\frac{\partial P}{\partial y} + \frac{1}{\rho_o}[\nabla\cdot\mu\nabla v + \frac{\partial \vec{v}}{\partial y}\cdot\nabla\mu] \quad (2)$$

$$\frac{Dw}{Dt} = - \frac{1}{\rho_o}\frac{\partial P}{\partial z} + \frac{1}{\rho_o}[\nabla\cdot\mu\nabla w + \frac{\partial \vec{v}}{\partial z}\cdot\nabla\mu] \quad (3)$$

Equation (1-3) may be expressed in vector notation

$$\frac{D\vec{v}}{Dt} = - \frac{1}{\rho_o}\nabla P + \vec{g}\beta(T-T_o) + \frac{1}{\rho_o}[(\nabla\cdot\mu\nabla)\vec{v} + \nabla\vec{v}\cdot\nabla\mu] \quad (4)$$

The last term in bracket $\nabla\vec{v}\cdot\nabla\mu$ may be neglected. Then

$$\frac{D\vec{v}}{Dt} = - \frac{1}{\rho_o}\nabla P + \vec{g}\beta(T-T_o) + \frac{1}{\rho_o}(\nabla\cdot\mu\nabla)\vec{v} \quad (5)$$

Here, the glass melts are considered as a pure viscous, incompressible flow. In order to allow the buoyancy force, however, the usual Boussinesq Approximation (12) is applied. That is, the density variation is neglected except they are coupled with gravity in the buoyancy force. Thus the fluctuations in density which appear with occurrence of motion result principally from thermal (as opposed to pressure) effects. This does not result from the Boussinesq approximation. The equation of state required is expressed

$$\rho = \rho_o\,[1-\beta(T-T_o)] \quad (6)$$

where β is the coefficient of volumetric expansion and the subscripts o denote a property at reference temperature

T_o. The viscosity of the glass melt is highly temperature dependent. Experimental data of the glass are usually correlated by the following relationship

$$\mu = \mu_o \exp E\left(\frac{1}{T} - \frac{1}{T_o}\right) \tag{7}$$

Continuity Equation: For incompressible flow,

$$\nabla \cdot \vec{v} = 0 \tag{8}$$

Energy Equation: The viscous dissipation may be neglected and the effective average thermal conductivity may be used with the Rosseland diffusion approximation.

$$\rho_o c_p \frac{DT}{Dt} = k_{eo} \nabla^2 T \tag{9}$$

Normalization of Equations

The above equations (1-5) may be normalized with the following dimensionless variables:

$$x^* = x/H \qquad y^* = y/H \qquad z^* = z/H$$

$$u^* = \frac{uH}{\alpha_{eo}} \qquad v^* = \frac{vH}{\alpha_{eo}} \qquad w^* = \frac{wH}{\alpha_{eo}} \; ; \; \vec{v}^* = \frac{\vec{v}H}{\alpha_{eo}} \tag{10}$$

$$p^* = \frac{pH^2}{\mu \alpha_{eo}} \qquad \nu^* = \frac{\nu}{\nu_o} \qquad t^* = \frac{t\alpha_{eo}}{H^2} \qquad \theta = \frac{T}{T_R}$$

$$\nabla^* = H\nabla$$

where $$\alpha_{eo} = \frac{k_{eo}}{\rho_o c_p} \tag{11}$$

The dimensionless equations are reduced to:

Momentum Equation

$$\frac{1}{Pr}\frac{D\vec{v}^*}{Dt^*} = \vec{R}_A(\theta-\theta_o) - \nabla^*P^* + \nabla^*\nu^*\nabla^*\vec{v}^* \qquad (12)$$

where

$$Pr = \frac{\mu_o c_p}{k_{eo}}$$

$$\vec{R}_A = \frac{\beta H^3 Tr\vec{g}}{\alpha_{eo}\nu_o}$$

Continuity Equation

$$\nabla^*\vec{v}^* = 0 \qquad (13)$$

and

Energy Equation

$$\frac{D\theta}{Dt^*} = \nabla^2\theta \qquad (14)$$

If we are interested in the two-dimensional solution only, the most effective way to solve the equations is to eliminate the pressure term. This can be accomplished by taking the curl of equation (11), and then taking the scalar component of the result.

Vorticity Equation

$$\frac{1}{Pr}\frac{D\omega^*}{Dt^*} = R_A\frac{\partial\theta}{\partial y^*} + \nabla^*\nu^*\nabla^*\ \omega^* \qquad (15)$$

where w is the vorticity defined as:

$$-\omega = \frac{\partial u}{\partial y} - \frac{\partial v}{\partial x} \tag{16}$$

The continuity equation can automatically be satisfied by introducing the stream function:

$$u = \frac{\partial \psi}{\partial y} \qquad v = -\frac{\partial \psi}{\partial x} \tag{17}$$

Poisson's Equation relates the stream function with vorticity

$$\nabla^2 \psi = -\omega \tag{18}$$

In dimensionless form, these are given by

$$\omega^* = \frac{\omega H^2}{\alpha_{eo}} \qquad \psi^* = \frac{\psi}{\alpha_{eo}} \tag{19}$$

Finally, the biharmonic equation may be obtained by substituting Poisson's equation into the vorticity transport equation.

$$\frac{1}{Pr}\frac{D}{Dt^*}(\nabla^{*2}\psi^*) = -R_a \frac{\partial \theta}{\partial y^*} + \nabla^* \nu^* \nabla^* (\nabla^{*2}\psi^*) \tag{20}$$

The solution of coupled equations (9) and (16) with appropriate initial and boundary conditions will represent the temperature field and stream function field.

The above coupled equations are solved by computer program CONRAD. The basic method of solution is to cast the problem as a transient initial value problem and extend the solution to steady-state. Since only the steady state results are of interest, choice of initial conditions is arbitrary (4). For this purpose, both motionless isothermal

initial conditions ($\psi=0$, $T=T_o$) or the results of a previous computer run are used to start the calculations (i.e. $\psi=f(x,y)$, $T=g(x,y)$). Completion of the problem statement requires a set of boundary conditions for both ψ and T. Presented in Table I are the hydrodynamic and thermal boundary conditions investigated in this thesis. The physical descriptions can be expressed in terms of the following equations:

No slip condition	ψ = constant	$\frac{\partial \psi}{\partial n} = 0$	(21)
Shear free surface	ψ = constant	$\frac{\partial^2 \psi}{\partial n^2} = 0$	(22)
Specified Temperature	$T = T_s$		(23)
No heat flux	$\frac{\partial T}{\partial n} = 0$		(24)
Specified heat flux	$- k \frac{\partial T}{\partial n} = q_F$		(25)
Specified heat transfer coefficient	$- k \frac{\partial T}{\partial n} = U(T-T_A)$		(26)

where $\vec{n}$ is the inward normal. Dimensionless heat flux and heat transfer coefficients are defined:

$$q_F^* = \frac{qH}{k_{eR}T_R} \tag{27}$$

and

$$N_u = \frac{UH}{k_{eR}} \tag{28}$$

to obtain the dimensionless analogs to these boundary conditions.

TABLE I. Boundary Conditions for Melting Chamber

(a) Hydrodynamic Boundary Conditions

	Boundary Region	Physical Description
(1)	All the walls and batch cover region	No slip condition
(2)	Symmetry line and flame region	Shear free condition

(b) Thermal Boundary Conditions

	Boundary Region	Physical Description
(1)	Batch cover region	Specified temperature
(2)	Symmetry line	No heat flux
(3)	Flame region	Specified heat flux
(4)	All the walls	Specified heat transfer coefficient (or Nusselt number) and ambient temperature

C. Source-Sink Approximation Method

One of the possible ways to solve the above three dimensional differential equations, of course, would be to attack the primitive equations. However, if accurate temperature and flow distributions are required, then a detailed mesh must be used to resolve the boundary layer region. This would make the cost of the solution prohibitively large, even with today's fast digital computers.

An obvious remedy is to make some simplifications to reduce the complexity and to obtain more ready solutions with reasonable accuracy. In this context, this thesis attempts to obtain a three-dimensional solution by solving more tractable equivalent two-dimensional problems. In doing so, an intrinsic difficulty is encountered in the modelling of the effect of the third dimension on the two-dimensional equations. This difficulty may be partially circumvented by introducing some sources-sinks functions of energy to model the transport in the third dimension. In the subsequent section, the method used to obtain the source-sink functions will be described.

The transient three-dimensional energy and continuity equations are in dimensionless form (drop the star sign)

$$\frac{\partial \Theta}{\partial t} + \frac{\partial U\Theta}{\partial x} + \frac{\partial V\Theta}{\partial y} + \frac{\partial W\Theta}{\partial z} = \frac{\partial^2 \Theta}{\partial x^2} + \frac{\partial^2 \Theta}{\partial y^2} + \frac{\partial^2 \Theta}{\partial z^2} \qquad (1)$$

and

$$\frac{\partial U}{\partial x} + \frac{\partial V}{\partial y} + \frac{\partial W}{\partial z} = 0 \qquad (2)$$

For the longitudinal section (x-y plane), two-dimensional equations can be written with appropriate source sink function, Φ :

$$\frac{\partial \theta}{\partial t} + \frac{\partial u\theta}{\partial x} + \frac{\partial v\theta}{\partial y} = \frac{\partial^2 \theta}{\partial x^2} + \frac{\partial^2 \theta}{\partial y^2} + \Phi \qquad (3)$$

and

$$\frac{\partial u}{\partial x} + \frac{\partial v}{\partial y} = 0 \qquad (4)$$

Since we have no a priori knowledge of the source-sink function Φ, this function must be estimated as a first approximation. The side wall heat losses may be considered as distributed point heat sinks throughout the furnace volume. Thus, for a uniform distribution:

$$\Phi = \frac{Q_{sw}}{HxWxL} \quad \frac{H^2}{k_e T_r} = \frac{2q^*_{sw}}{A_T} \qquad (5)$$

With the proper boundary conditions, the temperature and flow distribution, T and $\vec{v}$ can be obtained.

If we consider perturbations in the temperature and velocity in the transverse section (x-z plane), $\delta\vec{v}$ and δT, about the longitudinal section, we may write

$$\vec{V}(x,y_o,z) = \vec{v}(x,y_o) + \delta\vec{v}(x,z) \qquad (6)$$

$$\Theta(x,y_o,z) = \theta(x,y_o) + \delta\theta(x,z) \qquad (7)$$

The equation (6) may be expressed with vector components as:

$$\vec{V}(x,y,z) = \underline{i}U + \underline{j}V + \underline{k}W$$

$$= \underline{i}(u+\delta u) + \underline{j}v + \underline{k}\delta w \qquad (8)$$

Now, on substituting the components of velocity in equation (8) for the equation (2) and using the continuity equation (4) for longitudinal section, we obtain

$$\frac{\partial \delta u}{\partial x} + \frac{\partial \delta w}{\partial y} = 0 \qquad (9)$$

On substituting the equations (7) and (8) into energy equation (1), we obtain:

$$\frac{\partial}{\partial t}(\theta+\delta\theta) + \frac{\partial}{\partial x}[(u+\delta u)(\theta+\delta\theta)] + \frac{\partial}{\partial y}[v(\theta+\delta\theta)] + \frac{\partial}{\partial z}[\delta w(\theta+\partial\theta)]$$

$$= \frac{\partial^2}{\partial x^2}(\theta+\delta\theta) + \frac{\partial^2}{\partial y^2}(\theta+\delta\theta) + \frac{\partial^2}{\partial z^2}(\theta+\delta\theta) \qquad (10)$$

Subtracting the steady state solution of equation (3) from the equation (10) and manipulating with the two continuity equations (4) and (9), the equation desired to be solved for transverse section may be reduced to

$$\frac{\partial}{\partial t}(\theta+\delta\theta) + \frac{\partial}{\partial x}[\delta u(\theta+\delta\theta)] + \frac{\partial}{\partial z}[\delta w(\theta+\delta\theta)]$$

$$= \frac{\partial^2}{\partial x^2}(\theta+\delta\theta) + \frac{\partial^2}{\partial z^2}(\theta+\delta\theta) + SI_T \qquad (11)$$

where

$$SI_T = - \frac{\partial^2 \theta}{\partial x^2} - u \frac{\partial}{\partial x}(\delta\theta) - \Phi \qquad (12)$$

It is to be noted that δu and $\delta\theta$, as defined, are not functions of y. The first term of the source-sink function, SI_T, can be easily calculated from the longitudinal section temperature field. However, we do not know the term $u\frac{\partial}{\partial x}(\delta\theta)$ a priori and, indeed, we cannot explicitly solve it. If this term is to be incorporated into the program explicitly, it will lag behind the current iteration by one step. Furthermore, complications may arise from the specification of u values. According to the definition, they are the x-components of velocities in the longitudinal sections, which are orthogonal to a transverse section in question. They cannot be specified without further information on the various longitudinal section solutions. There seems to be no way to circumvent this difficulty in treating the source-sink approximation.

However, these velocity components should meet the no-slip condition on both of the side walls. As one moves from the centerline to the side wall, the velocity components are decreased to zero. Figure 5 shows the variation of normal velocity components (at y=o) for laminar flow in rectangular conduits (12). The velocities do not change greatly in the core region. For an aspect of

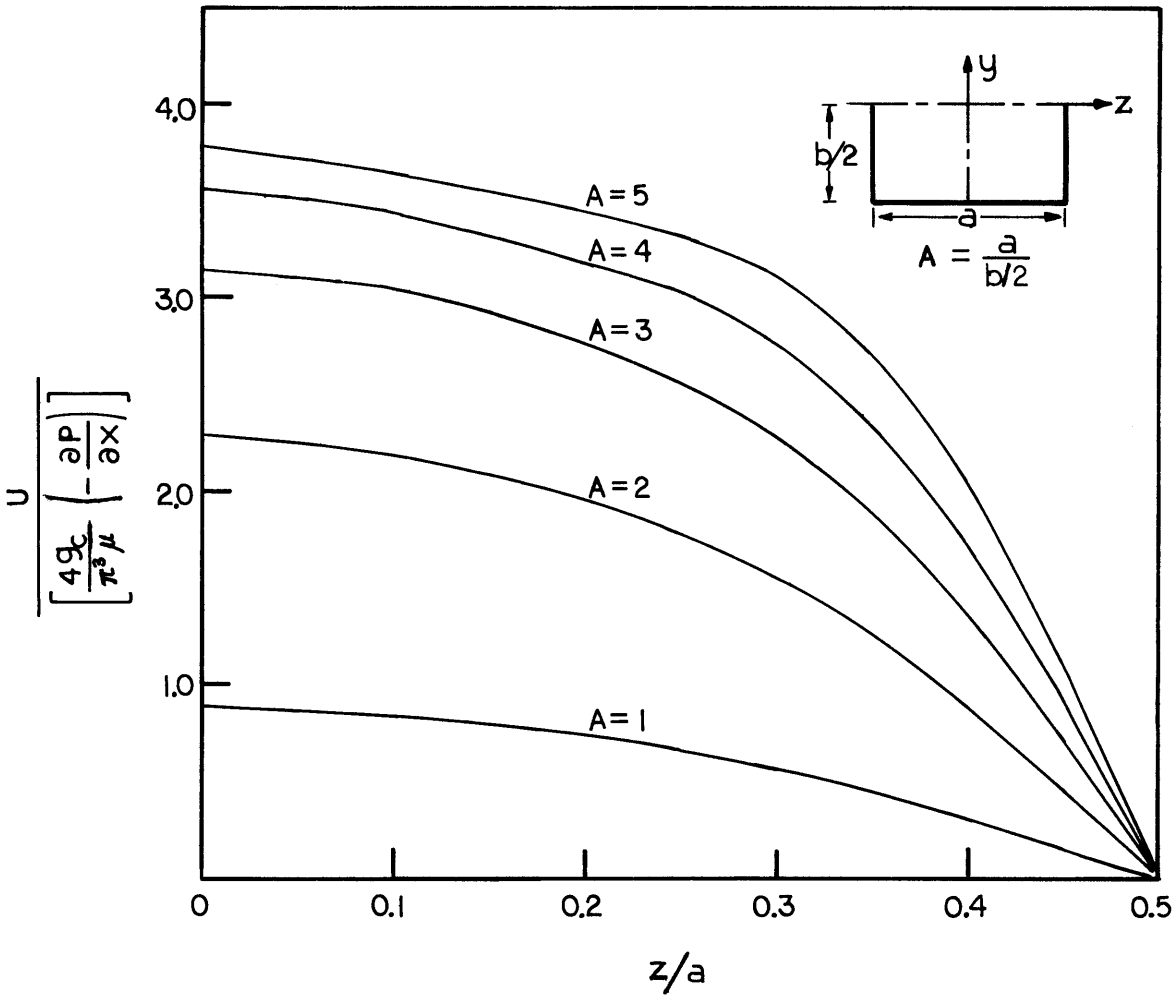

Figure 5. Normal Velocity Variation in a Rectangular Conduit

ratio 3, significant change occurs near the side wall. In the glass furnace, changes in the direction of u velocities over the entire transverse section will introduce another complication. Therefore, the inclusion of term $u \frac{\partial \delta \theta}{\partial x}$ may represent a refinement not warranted by approximations inherent in the source-sink method. We then drop this term. The equation becomes

$$SI_T = - \left. \frac{\partial^2 \theta}{\partial x} \right|_L - \Phi \qquad (13)$$

Before proceeding with the discussion of the construction of three-dimensional picture of the convection flow, it is desirable to examine carefully the limitations to be expected from the assumptions and approximations involved, explicitly or implicitly, in the above derivation. Foremost of these is the acceptance of additive contribution to the three-dimensionality from the two orthogonal two-dimensional motions. For other problems without this additive property, the whole concept of the stream function will cease to be of value so that the method cannot be applied.

One further assumption in this treatment, but not mentioned in the course of the preceding development, remains to be considered. This one is of a rather more subtle nature.

Incorporating the estimates of the effects of three-dimensional motion into the appropriate two-dimensional equations, it has been assumed that only the energy source-sinks are distributed essentially throughout the orthogonal plane, while the momentum source-sinks are not incorporated. Basically, the convection currents in the furnace are caused by the temperature gradient and the resulting difference in density. This is true for the transverse section as well as the longitudinal section. In other words, the thermal interactions between heat sources and sinks cause the momentum transfer. Furthermore, the momentum transfer can be expressed as a vector quantity which has three mutually independent components. Thus, the use of the appropriate temperature (not the perturbation temperature) in the momentum equation will satisfactorily incorporate the momentum source-sinks into the momentum equation.

Now turning to the problem of constructing the three-dimensional picture of convective flow, we will derive the source-sink functions for the longitudinal section. Since the temperature field and the stream function field can be obtained for any plane of transverse sections, the estimates of the effect of transverse section field on the longitudinal section does not pose any difficulties. From the results obtained for the various transverse sections, we can construct temperature and velocity fields corresponding to

any specified longitudinal section. That is

$$\theta'(x,y,z^\circ) = \theta(x,y) + \delta\theta(x,z^\circ) \tag{14}$$

$$\vec{v}'(x,y,z^\circ) = \vec{v}(x,y) + \delta\vec{v}(x,z^\circ)$$

$$= \underline{i}(u+\delta u) + \underline{j}v' + \underline{k}\,(\delta w) \tag{15}$$

where z° is the z coordinate corresponding to the chosen longitudinal section. Introducing perturbation terms in the x-y plane, $\delta\vec{v}'$ and $\delta\theta'$, we may write

$$\theta(x,y,z^\circ) = \theta'(x,y,z^\circ) + \delta\theta'(x,y) \tag{16}$$

$$\vec{V}(x,y,z^\circ) = \vec{v}'(x,y,z^\circ) + \delta\vec{v}'(x,y) \tag{17}$$

$$= \underline{i}(u+\delta u+\delta u') + \underline{j}(v+\delta v') + \underline{k}\,\delta w$$

Upon substituting equation (17), the continuity equation can be written

$$\frac{\partial}{\partial x}(u+\delta u+\delta u') + \frac{\partial}{\partial y}(v+\delta v') + \frac{\partial\,\delta w}{\partial z} = 0 \tag{18}$$

which reduces to

$$\frac{\partial(u+\delta u')}{\partial x} + \frac{\partial(v+\delta v')}{\partial y} = 0 \tag{19}$$

according to the equation (9).

At the steady state, the equation (11) with new notation can be written

$$\frac{\partial}{\partial x}(\delta u\theta') + \frac{\partial}{\partial z}(\delta w\theta') = \frac{\partial^2\theta'}{\partial x^2} + \frac{\partial^2\theta'}{\partial z^2} + SI_T \tag{20}$$

Substituting equation (16) and (17) into (1) and subtracting eq. (20) from it, we may obtain energy equation in the form of

$$\frac{\partial}{\partial t}(\theta'+\delta\theta') + \frac{\partial}{\partial x}(u+\delta u')(\theta'+\delta\theta') + \frac{\partial}{\partial y}(v+\delta v')(\theta'+\delta\theta')$$

$$= \frac{\partial^2}{\partial x^2}(\theta'+\delta\theta') + \frac{\partial^2}{\partial y^2}(\theta'+\delta\theta') + SI_L \qquad (21)$$

where

$$SI_L = - \left.\frac{\partial^2\theta'}{\partial x^2}\right|_T - SI_T \qquad (22)$$

neglecting $- \delta u \frac{\partial}{\partial x} (\delta\theta')$ term.

Equation (22) provides the effect of the transverse section flow on the longitudinal flow. Furthermore, with the results obtained from eq. (21), we may further refine the ϕ terms in equation (3). In this way, the temperature and stream function field can be refined, within the limitation of this approximation model.

Finally, the differential equations for source-sink approximation method is summarized in Table II. The inspection of energy equations shows that the common form to be solved is:

$$\frac{\partial\theta}{\partial t} + \frac{\partial(u\theta)}{\partial x} + \frac{\partial(v\theta)}{\partial y} = \frac{\partial^2\theta}{\partial x^2} + \frac{\partial^2\theta}{\partial y^2} + SI(x,y) \qquad (23)$$

which is the same form exactly as the energy equation that CONRAD program can handle.

A brief description of the CONRAD program can be found in Appendix A.

TABLE II. Differential Equations for Source-Sink Approximation

1. Longitudinal Section (Center Line)

Continuity: $$\frac{\partial u}{\partial x} + \frac{\partial v}{\partial y} = 0$$

Energy: $$\frac{\partial \theta}{\partial t} + \frac{\partial (u\theta)}{\partial x} + \frac{\partial (v\theta)}{\partial y} = \frac{\partial^2 \theta}{\partial x^2} + \frac{\partial^2 \theta}{\partial y^2} + \Phi$$

2. Transverse Sections

Continuity: $$\frac{\partial \delta u}{\partial x} + \frac{\partial \delta w}{\partial z} = 0$$

Energy: $\theta' = \theta + \delta\theta$

$$\frac{\partial \theta'}{\partial t} + \frac{\partial (\delta u \theta')}{\partial x} + \frac{\partial (\delta w \theta')}{\partial z} = \frac{\partial^2 \theta'}{\partial x^2} + \frac{\partial^2 \theta'}{\partial z^2} + SI_T$$

Source-Sink Function $$SI_T = - \left.\frac{\partial^2 \theta}{\partial x^2}\right|_L - \Phi$$

3. Longitudinal Sections

Continuity: $$\frac{\partial (u+\delta u')}{\partial x} + \frac{\partial (v+\delta v')}{\partial y} = 0$$

Energy: $\theta'' = \theta' + \delta\theta'$

$$\frac{\partial \theta''}{\partial t} + \frac{\partial [(u+\delta u')\theta'']}{\partial x} + \frac{\partial [(v+\delta v')\theta'']}{\partial y} = \frac{\partial^2 \theta''}{\partial x^2} + \frac{\partial^2 \theta'}{\partial y^2} + SI_L$$

Source-Sink Function $$SI_L = - \left.\frac{\partial^2 \theta'}{\partial x^2}\right|_T - SI_T$$

Biharmonic Equation* $$\frac{1}{N_{Pr}} \left| \frac{\partial \nabla^2 \psi}{\partial t} + \frac{\partial}{\partial x}(u\nabla^2\psi) + \frac{\partial}{\partial y}[v\nabla^2\psi] \right| = -N_{RA} \frac{\partial \theta}{\partial y} + \frac{\partial}{\partial x}\left(\mu \frac{\partial \nabla^2 \psi}{\partial x}\right) + \frac{\partial}{\partial y}\left(\mu \frac{\partial \nabla^2 \psi}{\partial y}\right)$$

*Appropriate velocity components and coordinate system should be used in conjunction with the above energy equation (e.g. for transverse sections, u,v,y are replaced with $\delta u, \delta w$ and z respectively.

IV. NUMERICAL CASE STUDY

This chapter provides a description of each of the pertinent numerical runs made in the course of this investigation. To demonstrate the capability of the source-sink approximation method, a test case was first run with a Rayleigh number, 10^7, corresponding to the industrial glass furnace. This test case was chosen so that they compared with the Clomburg results for a Rayleigh number of 10^6, all other parameters being constant. Since there exist no appropriate experimental data, a scaling law was developed to compare the two results.

Next, an extensive application of this method was attempted to a problem with non-dimensional parameters of interest to industrial glass furnace operation. The prototype actually modelled is related to a green glass furnace to retain the salient aspects of an industrial glass furnace.

A. Test Case

Numerical results demonstrating the capability of the source-sink approximation method are presented. Clomburg (4) carried out several numerical runs for the transverse section to investigate the effect of thermal boundary conditions on the flow patterns with Rayleigh Number ~10^6. The effects of bottom and side wall heat transfer coefficients and internal heat generation or removal were investigated. His numerical runs were repeated with an increased Rayleigh number, 10^7. The geometry and boundary conditions are shown

in Figure 6. The dimensionless parameters common to both cases are listed in Table III. The transverse section is made somewhere in the open area of a furnace, that is, not under the batch cover. Energy supplied through the top surface at a specified rate provides energy for the heat losses through the sides and bottom (heat transfer coefficient, Nu, and ambient temperature, θ_A, specified), and also for the enthalpy gains (i.e. source-sink functions) of material being heated as it passes through the plane of the figure in the third dimension. For these runs, the no slip hydrodynamic boundary condition is used.

TABLE III. Summary of Common Parameters for Test Runs

System Parameters	A	N_{RC}	$N_{PR} \times 10^{-2}$	N_{vis}	$\theta_{ambient}$		
Value	2.0	0	4.85	13.5	.189		
Run Number	**I**	**II**	**III**	**IV**	**V**	**VI**	**VII**
Wall Nusselt #, N_{Nu_w}	.0275	.0275	.0546	.0275	.0275	.0275	.0546
Bottom Nusselt #, N_{Nu_B}	.1340	.1340	.1340	0.0	0.0	0.0	0.0
Top Heat Flux, q*	.1305	.2618	.2841	.0223	.0723	.0723	.0443
Internal generation rate (average) Φ	0.0	-.1309	-.1309	0.0	-.05*	-.05	0.0

*A linear distribution with depth was assumed, i.e. ϕ is +0.02 at the surface and -0.12 at the bottom.

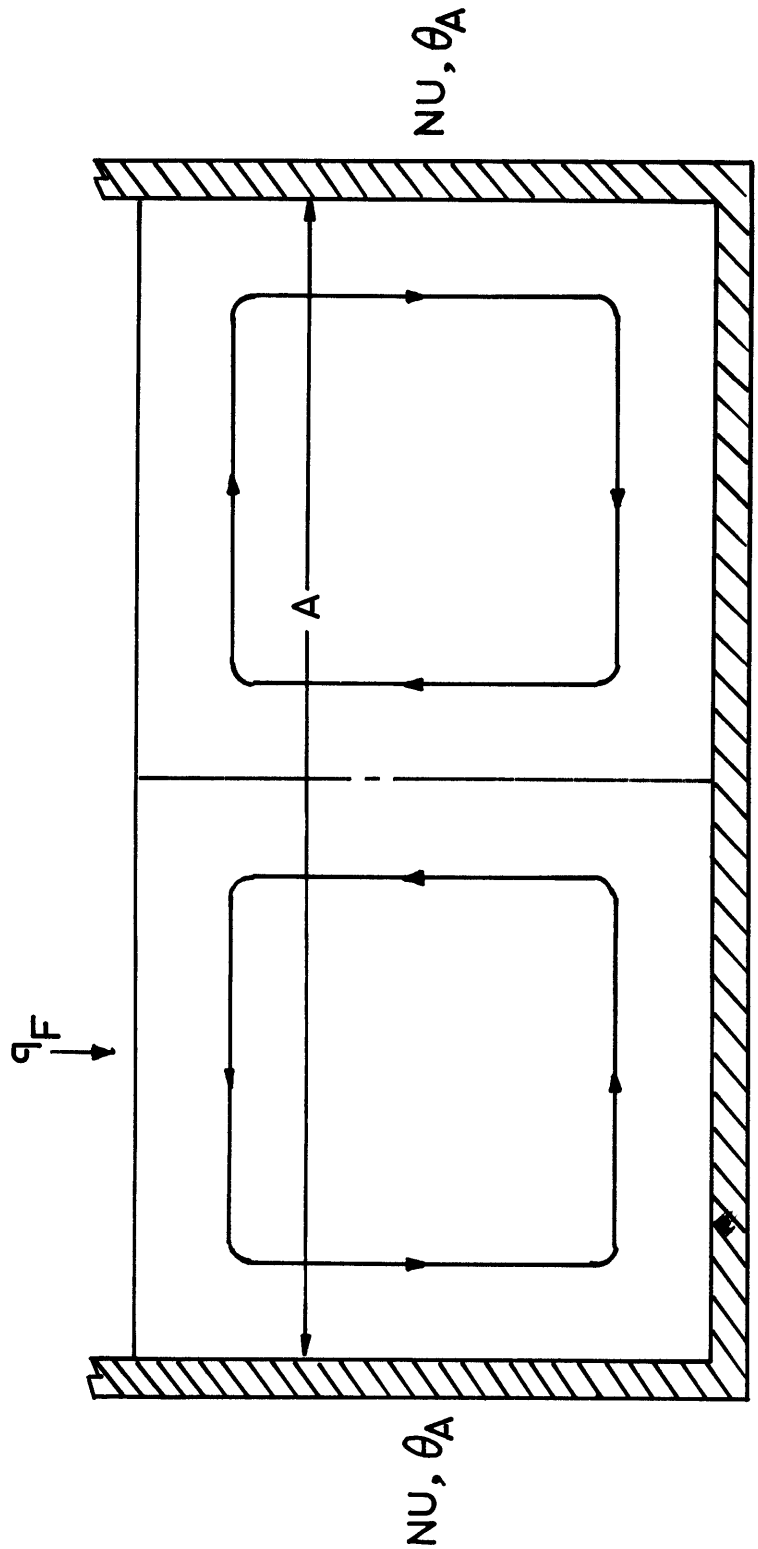

Figure 6. Geometry for Test Case

Because of the symmetry of the problem it is necessary to carry out the calculation for one-half of transverse section only.

A grid with uniform spacing is not satisfactory in problems with boundary layers (15). In order to have the number of points large enough to resolve the boundary layer (at least three points in it) (11, 16). A non-uniform grid was obtained from the stretched coordinate system. For the present problem, the selected stretched coordinate systems are

$$x = \sin^2\left(\frac{\pi}{2}\,\xi\right) \quad \text{for x direction} \tag{1}$$

and

$$z = \eta^2 \quad \text{for z direction} \tag{2}$$

Equation (1) is symmetrical about ξ=0.5. It is a convenient stretched coordinate, when a boundary layer is expected at both x=0 and x=1 (i.e. one at the top surface and the other at the bottom of the furnace). The grid system thus obtained is the nonuniform 15×16 grids, which is in contrast to the 10×20 uniform grid (10×10 grid for half plane) employed in Clomburg's case. More often than not, oscillating stream lines and isotherms were obtained when the coarse, irregular net was employed (14). Some authors (20) suspect that the computed flow pattern became much simpler when the solution was repeated with a uniform grid. Throughout the course of computation, the 15×16 grid system was employed for transverse section in order to suppress these types of

spurious effects.

During the execution of each run on the IBM 370 model 165, the calculations were terminated and the temperature and stream function field was punched out on deck cards after 200 iterations. Complete intermediate printout was obtained every 100 iterations with transient values at the maximum stream function point being calculated every iteration. Normally, rapid convergence was obtained after 150 iterations. To ensure a steady state attainment, computation was terminated when the following requirements were satisfied:

(1) temperature residual should be less than 10^{-2} or 10^{-3} throughout the field. The temperature residual is defined as

$$RT(I,J) = -\vec{V}\cdot\nabla\theta_{ij} + \nabla^2\theta_{ij} + S_{ij} \qquad (3)$$

In this way, the resulting energy balance always shows less than 0.5% closure of the heat input to the furnace.

(2) Transient temperature and stream function values should converge within an arbitrarily small range at or near the point of maximum stream function.

In some cases (usually with large bottom heat transfer coefficient), the requirements for percentage closure of energy balance was not satisfied after 200 iterations. In those cases, the punched output was put in as initial condition and the temperature field was advanced with the

flow field being frozen. Then the results obtained were again read in to solve the coupled energy and flow equation until the above requirements were satisfied.

The results are summarized in Table IV with Clomburg's case.

TABLE IV. Comparison of Test Case Results

Rayleigh Number	Clomburg's Case 10^6			This Study 10^7		
Grid System	10×10 uniform grid			15×16 Grid		
Run Number	Maximum θ	Minimum θ	Total Circulation	Maximum θ	Minimum θ	Total Circulation
I (636)*	1.061	.944	.249	1.098	.980	.303
II (641)	1.099	.924	.160	1.158	.975	.173
III (642)	1.105	.919	.301	1.162	.969	.335
IV (637)	1.008	.992	1.72	1.007	.993	2.81
V (639)	1.024	.984	.769	1.023	.986	1.269
VI (640)	1.029	.979	.534	1.029	.980	.815
VII (645)	1.015	.983	1.924	1.014	.987	3.078

*The numbers in parenthesis correspond to the run number in Clomburg's thesis.

The effect of the parameter changes appeared qualitatively similar to those reported by Clomburg. The results may be summarized:

(1) Effect of bottom heat loss: Relatively large bottom heat transfer coefficients (Runs I, II, III) have the effect of generating nearly horizontal isotherms, which tend to decrease the circulation rate. In these cases, the increased Rayleigh number raises the temperature throughout the field, though it does not show any significant change in the circulation rate compared to Clomburg's case. When the bottom is insulated, the circulation rate is increased, but the temperature distribution shows little change at all. (Runs IV, V, VI, VII). A scaling law derived on the basis of order of magnitude analysis can be used to estimate the circulation rates from the known results at different Rayleigh number (Appendix B).

(2) Internal heat absorption: Its existence tends to stabilize the flow (comparing Runs II and V with Run IV). The effect of linearly distributed sinks (RUN VI compared to V) shows that the circulation rate is decreased due to the higher removal of heat near the bottom. In the case of high internal absorption and high bottom losses (Run II, III) the circulation rate appears to be proportional to the side heat flux.

By and large, the contour plots of streamlines and temperature fields appeared similar in shape in both cases. It is instructive to compare the circulation rate to the estimated value from the known results at different Rayleigh numbers. Order of magnitude analysis (Appendix B) shows the

scaling law can be applied for the case of the bottom insulation (7):

$$\psi = \nu \frac{Ra^{1/4}}{Pr} = \alpha Ra^{1/4} \tag{4}$$

For the case under consideration, it may be written as

$$\frac{\psi_2}{\psi_1} = \left[\frac{Ra_2}{Ra_1}\right]^{1/4}$$

or $$\psi_2 = 1.778 \times \psi_1 \tag{5}$$

The estimated circulation rates are listed in Table V. Even though the effect of top heat fluxes are ignored in the course of derivation, a good agreement was obtained between the calculated and the estimated values.

TABLE V. Comparison of Calculated and Estimated Circulation Rate

Run Number	ψ_{max}, Calculated		ψ_{max}, Estimated	$\psi_{cal}/\psi_{est.}$
	$Ra=10^6$	$Ra=10^7$		
IV	1.72	2.81	3.06	.92
V	.769	1.269	1.37	.93
VI	.534	.815	.95	.86
VII	1.924	3.078	3.42	.90

B. Simulation of Green Glass Furnace

In this section, an extensive application of the method is presented. To retain the salient aspects of an industrial

glass furnace, the modelled prototype is closely related to a green glass furnace. Ideally, a complete, three-dimensional model of a glass furnace should be geometrically and dynamically similar to the prototype. However, complete duplication of the prototype is an unattainable task. Thus we are forced to seek a compromise between practicability and exactness. According to suggested simplification (4), the following assumptions were made:

(1) The circulation of glass melts in furnaces are considered as those of a purely viscous fluid in a rectangular enclosure. Therefore the effect of bubbles and chemical reaction will be neglected. Furthermore, no fluid throughput is permitted for simplicity.

(2) The radiative heat transfer is described with an "effective" thermal conductivity according to the Rosseland diffusion equation (9).

(3) The temperature dependence of properties are only applied to the density and the viscosity.

(4) The flame-side and the melt-side energy transfer are decoupled. The batch-cover, as a plane of extent L, is maintained at specified sink temperature T_s, representing the bottom surface temperature of the batch. The flame side radiation is idealized by a specified energy flux, q_F^*. However, these simplifications may be refined to allow the spatially distributed temperature and energy flux.

(5) The end walls and bottom of the furnace are assumed

to lose heat to a sink at temperature T_A. Therefore the overall heat transfer coefficient U will be used.

1. Evaluations of Parameters

With the above simplifications, the relevant physical properties and dimensions for the green glass furnace are listed in Table VI. For nondimensionalizing the equations and evaluating the physical properties, the reference temperature was selected at an intermediate temperature between the maximum and minimum values prevailing in the furnace. At the batch cover, the temperature assumes somewhat higher value than the melting temperature of raw materials. The relevant physical properties are calculated based on the available experimental data.* The viscosity is highly temperature dependent. The experimental data shown in Figure 7 may be expressed in compact form.

$$\mu = \mu_o e^{E(1/T-1/T_o)} \tag{6}$$

The variation of density with temperature was assumed to be linear.

$$\rho = \rho_o [1-\beta(T-T_o)] \tag{7}$$

The experimental data, as shown in Figure 8, is well fitted with $\beta=2.75\times10^{-5}{}^\circ R^{-1}$.

Next, the effective thermal conductivity is calculated following the procedure by Hottel and Sarofim (9).

*From the private communication of N.W.E. Curlet with R. L. Curran.

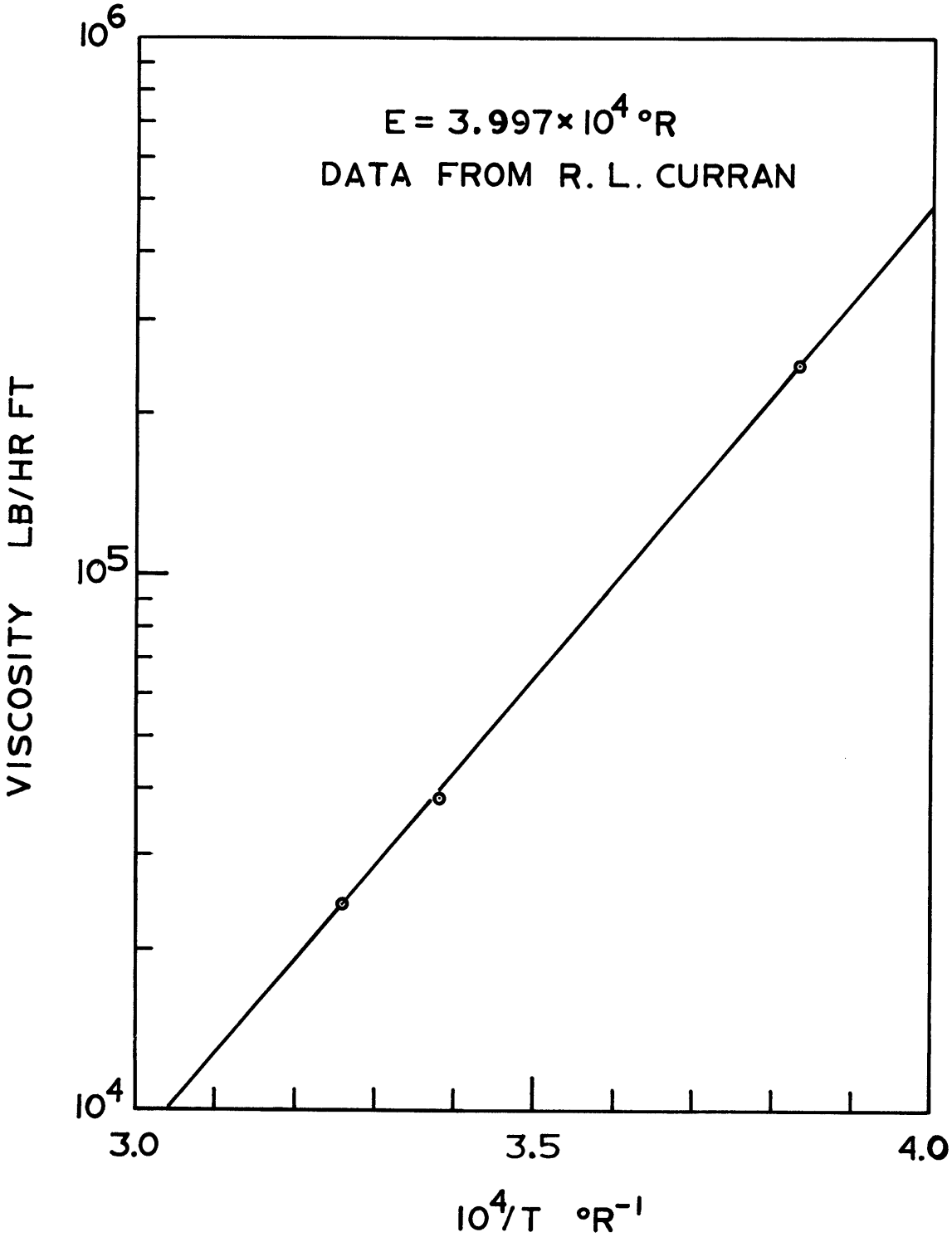

Figure 7. Viscosity of Green Glass Versus Temperature

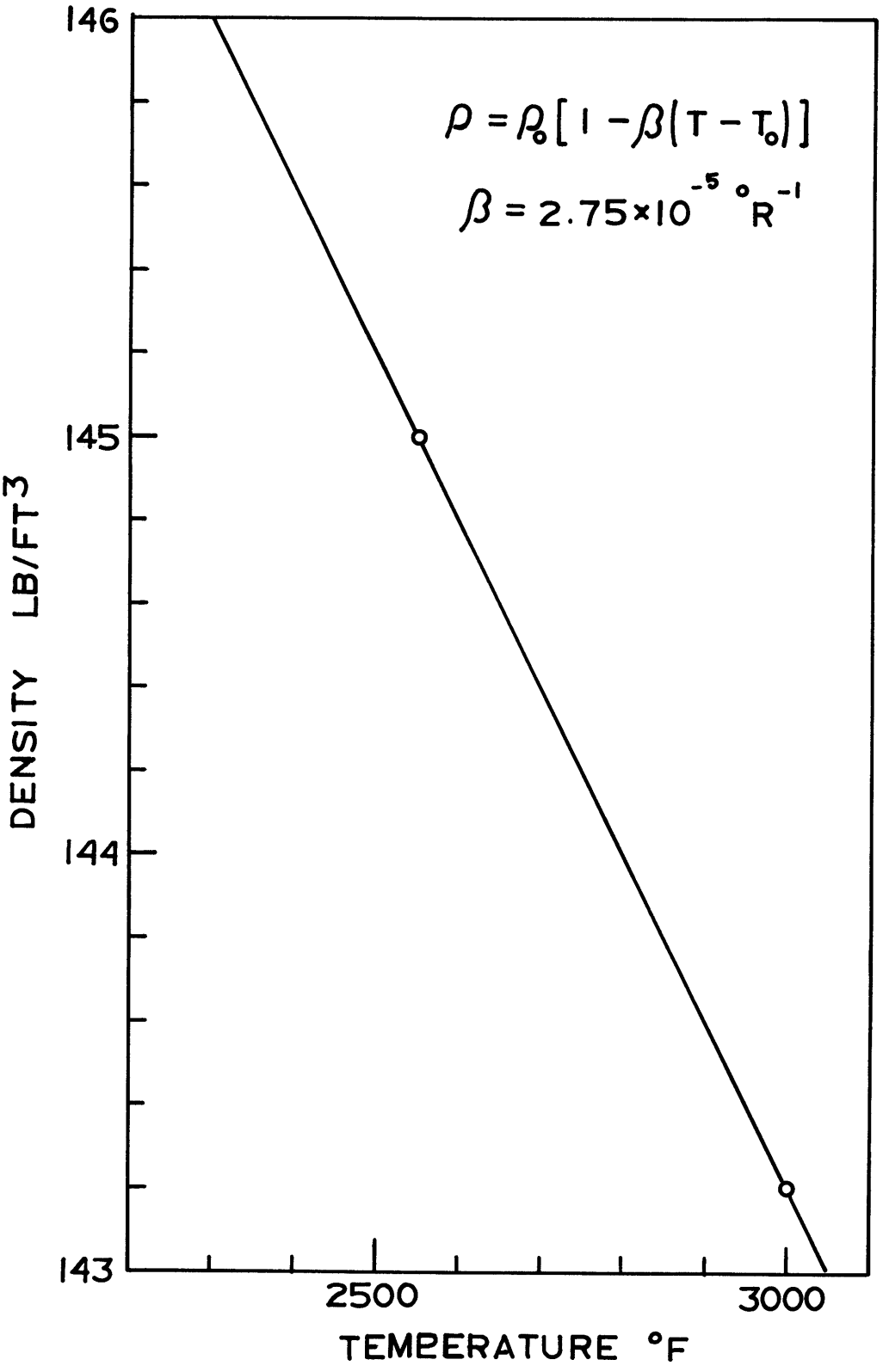

Figure 8. Density of Green Glass Versus Temperature

TABLE VI. Dimensions and Properties of Green Glass Furnace

Dimensions:		
H	Height of furnace	3 3/4 ft
L	Length of furnace	22 1/2 ft
W	Width of furnace	11 1/4 ft
B	Length of Batch coverage	11 1/4 ft
Properties:		
T_o, T_R	Reference temperature for properties	2500°F (2960°R)
T_A	Ambient temperature	100°F
T	Effective batch temperature	2785°R
μ_o	Viscosity	3.841×10^4 $\frac{lb}{ft\ hr}$
E	Viscosity variation coefficient	3.997×10^4 °R
ρ_o	Density	145.2 lb/ft^3
β	Volumetric expansion coefficient	2.75×10^{-5}/°R
c_p	Heat capacity	0.39 Btu/lb°R
k	Thermal conductivity	0.7 Btu/hr ft°R
k_e	Effective thermal conductivity	9.0 Btu/hr ft°R
Heat Transfer Coefficients at:		
Bottom	U_B	0.138 Btu/hr ft^2°F
Bridgewall	U_{BW}	4.0 Btu/hr ft^2°F
Doghouse wall	U_{DW}	1.11 Btu/hr ft^2°F
Side walls	U_{SW}	0.4566 Btu/hr ft^2°F

The radiative heat transfer coefficients are obtained using the Rosseland mean absorption coefficients from the equation

$$k_{rad} = \frac{16\eta^2\sigma T^3}{3} \int_0^1 \frac{1}{K_\lambda} df^* \tag{8}$$

where

$$f^* = \int_0^1 \left(\frac{\partial E_\lambda}{\partial E}\right)_\lambda d\lambda \tag{9}$$

The function f* is given in terms of $\lambda T/C_2$ as shown in Figure 9. If the relationship between the absorption coefficient (K) and the wavelength (λ) is expressed as a number of discrete step functions, the effective radiative conductivity may be calculated

$$k_{rad} \simeq \frac{16\eta^2\sigma T^3}{3} \sum_i (f_i^* - f_{i-1}^*)/K_i \tag{10}$$

Experimental absorption coefficients data at 1623°K (with η = 6.35 mm) are also plotted against the wavelength in Figure 10. From these data, the summation terms amount to 0.475. Thus,

$$k_{rad} = \frac{16}{3} (1.52)^2 (1623)^3 (1.356) (0.475) \tag{11}$$

$$= 0.0339 \text{ cal/cm sec °C}$$

$$= 8.2 \text{ Btu/hr ft°F}$$

Finally, the effective thermal conductivity is calculated by summing the true thermal conductivity and the radiative conductivity. Therefore

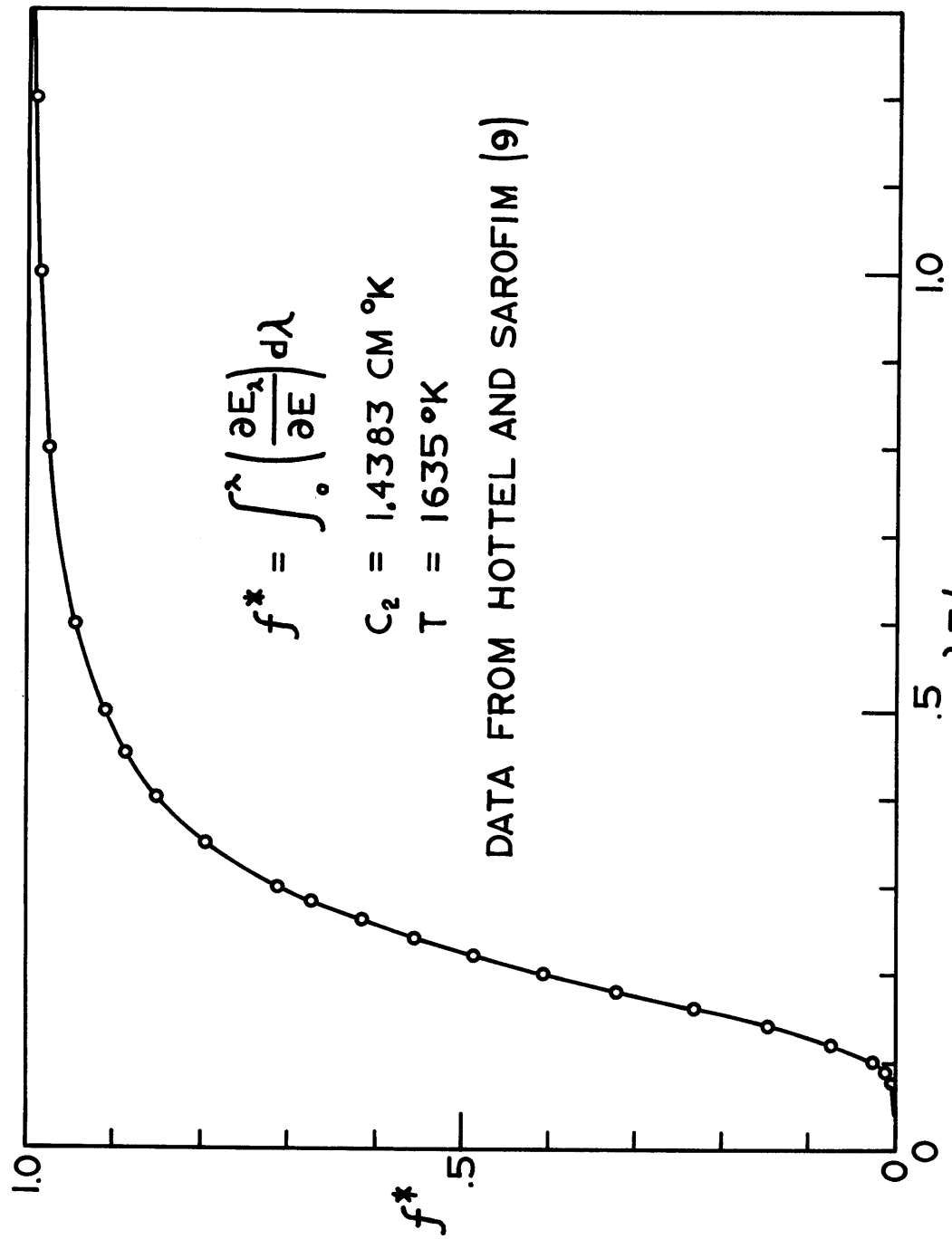

Figure 9. Plot of f* versus $\lambda T/c_2$

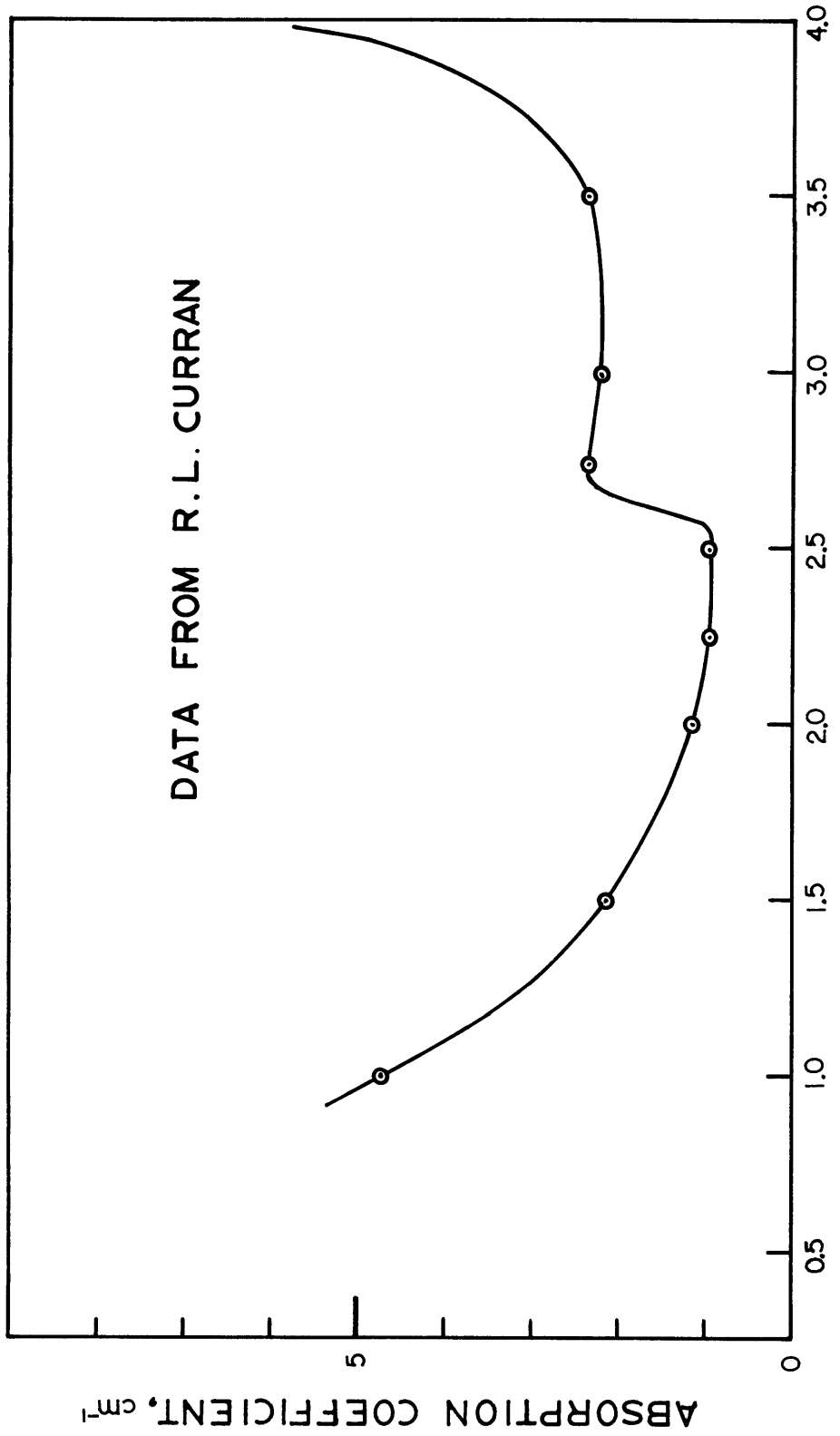

Figure 10. Spectral Absorption Coefficient for Emerald Green Glass

$$k_e = k + k_{rad} \tag{12}$$

$$= 8.9 \sim 9 \text{ Btu/hr ft } °F$$

The nomenclature of the preceding equation is that of Hottel and Sarofim (9).

Heat loss to the ambient can be expressed in general form

$$Q = \frac{T_i - T_o}{\ell/k} = h_{CR} (T_o - T_A) \tag{13}$$

where T_i, T_o and T_A are the inner wall, the outer wall and ambient temperatures, respectively, and ℓ and k denote wall thickness and its thermal conductivity, respectively. The empirical relation exists for the radiation and conduction heat transfer coefficient, h_{CR} :

$$h_{CR} = 0.22 (T_o - T_A)^{1/3} + 4\sigma \left(\frac{T_o + T_A}{2}\right)^3 \tag{14}$$

where σ is the Stefan-Boltzmann constant, 1.714×10^{-9} Btu/ft^2°R^{4}hr. The overall heat transfer coefficients are readily obtained by combining above two equations.

$$u = \frac{Q}{T_i - T_A} \tag{15}$$

The boundary heat transfer coefficient listed in Table VI are determined from wall construction and wall temperature measurements following the procedure described above. It is assumed that 10 per cent of the heat supplied is lost through the side walls.

From the furnace data and the physical properties of the glass in Table VI, the dimensionless parameters and boundary conditions which are required for the numerical algorithm were calculated. These are shown in Table VII. The heat source from the flame side is a uniform flux to the top surface and is considered as the sum of the heat losses to the batch and the heat losses to the various walls and bottom. ($Q=1.695\times10^6$ Btu/hr).

2. Numerical Run for Longitudinal Section

It is implicitly assumed that the transverse section convective flows are a pertubation of those in the longitudinal section. Therefore it is logical to obtain the longitudinal section flow patterns prior to the application of the source-sink method to the problem. In doing so, the evaluation of Φ term is required. As already mentioned, this term was specified as the uniformly distributed point heat sinks through the longitudinal section.

$$\text{Thus,} \quad \Phi = \frac{2q^*_{sw}}{A_T} = 0.09427 \tag{16}$$

where ten percent of the heat supplied from the flame side is assumed to be lost through both the side walls. Examination of this assumption reveals that the longitudinal section results obtained in this way may represent the centerline section at most.

TABLE VII. Dimensionless Parameters for the Green Glass Furnace

Parameters		Definition	Value
Rayleigh Number, Ra		$\frac{g\beta H^3 T_R}{\nu_R \alpha_{eR}}$	4.26×10^7
Prandtl Number, Pr		$\mu_R C_p / k_{eR}$	1.66×10^3
Nusselt Number, Nu		UH/k_{eR}	
at Bottom	Nu_B		0.0575
Bridgewall	Nu_{BW}		1.666
Doghouse wall	Nu_{DW}		0.4625
Side walls	Nu_{SW}		0.19025
Viscosity Number,	N_v	E/T_R	13.5
Ambient Temperature,	θ_A	T_A/T_R	0.189
Heat flux to top,	q^*_F	$qH/k_{eR}T_R$	1.8854
Batch Temperature,	θ_s	T_s/T_R	0.9409
Aspect Ratio, A			
Longitudinal Section	A_L	L/H	6
Transverse Section	A_T	W/H	3
Batch Coverage, C		B/L	0.5
Reference Temperature		$T_R=T_\theta$	2960°R

The boundary conditions are specified with C=0.5 and A_L=6.0.

$$y=0 \quad 0\leq x\leq 1 \quad \psi=\frac{\partial\psi}{\partial x}=\frac{\partial\psi}{\partial y}=0 \quad \frac{\partial\theta}{\partial y}=Nu_{DW}(\theta-\theta_A) \tag{17}$$

$$y=6 \quad 0\leq x\leq 1 \quad \psi=\frac{\partial\psi}{\partial x}=\frac{\partial\psi}{\partial y}=0 \quad -\frac{\partial\theta}{\partial y}=Nu_{BW}(\theta-\theta_A) \tag{18}$$

$$0\leq y\leq 3 \quad x=0 \quad \psi=\frac{\partial^2\psi}{\partial x^2}=\frac{\partial\psi}{\partial y}=0 \quad \theta=\theta_s \tag{19}$$

$$3\leq y\leq 6 \quad x=0 \quad \psi=\frac{\partial\psi}{\partial y}=\frac{\partial^2\psi}{\partial x^2}=0 \quad -\frac{\partial\theta}{\partial x}=q_F^* \tag{20}$$

$$0\leq y\leq 6 \quad x=1 \quad \psi=\frac{\partial\psi}{\partial x}=\frac{\partial\psi}{\partial y}=0 \quad -\frac{\partial\theta}{\partial x}=Nu_B(\theta-\theta_A) \tag{21}$$

Above, stream functions are arbitrarily chosen as zero at all points on the boundary. The second derivative of stream function in equation (20) was set to zero to represent shear free surface condition on flame side zone.

We expect rapid temperature variations at the two end walls and near the terminus of the batch cover along the top surface. This suggests some refined grid system in y should be used for these boundary layer zones. Since it is difficult to produce such grid systems by a stretched coordinate system, the irregular grid system in the x-direction was refined in the regions near the side walls and near the transition zones between the flame-side and the batch cover. The values Δx, Δy, and Δz used in this study are listed with the zone number in Table VIII. (The coordinate systems, Δy and Δz, were obtained by the stretched coordinate system.)

TABLE VIII. Zone Size Versus Zone Number

Number of Zones, * I		Δx(I) (M = 34)	Δy(I) (N = 15)	Δz(I) (K = 16)
1	(34)	0.002	.0192	.0078
2	(33)	0.004	.0377	.0156
3	(32)	0.006	.0547	.0234
4	(31)	0.008	.0696	.0313
5	(30)	0.01	.0819	.0391
6	(29)	0.02	.0910	.0469
7	(28)	0.03	.0966	.0547
8	(27)	0.04	.0986	.0625
7	(26)	0.04	.0966	.0703
10	(25)	0.05	.0910	.0781
11	(24)	0.05	.0819	.0859
12	(23)	0.05	.0696	.0938
13	(22)	0.05	.0547	.1016
14	(21)	0.05	.0377	.1094
15	(20)	0.04	.0192	.1172
16	(19)	0.03		.0624
17	(18)	0.02		

*Numbers in brackets represent the zone number in x-direction.

Results and Discussion

Computed isotherm and streamline maps are shown in Figure 11.

Except near the end walls and along the top surface, temperatures vary only slightly within the melt. The most extreme temperature gradients exist under the flame side where energy is absorbed by the convection currents, and under the batch where it is released to the cold input material. Significant temperature gradients also exist near the dog house wall (left hand side wall) and the bridge wall. The effects of side wall heat loss are twofold: first, the intrusion of the extreme temperature gradient under the batch cover is much depressed comparing to the results obtained without side wall heat loss Φ (cf. discussion of Clomburg (4) and (13)) and secondly, the horizontal temperature profiles show slight curvature as they approach the bottom. Without the side wall heat losses, this temperature profile is nearly stratified down to the bottom surface except the corner zone.

The stream function field indicates the flow pattern. Crowding of the streamlines denotes region of high velocity. The largest horizontal velocities occur in the terminus of the batch cover. As indicated from the isotherms, this region corresponds to thermal couple between the flame side and the batch sink on the top surface, which provides the principle driving force for the flow. This driving force is further enhanced by the heat loss through the

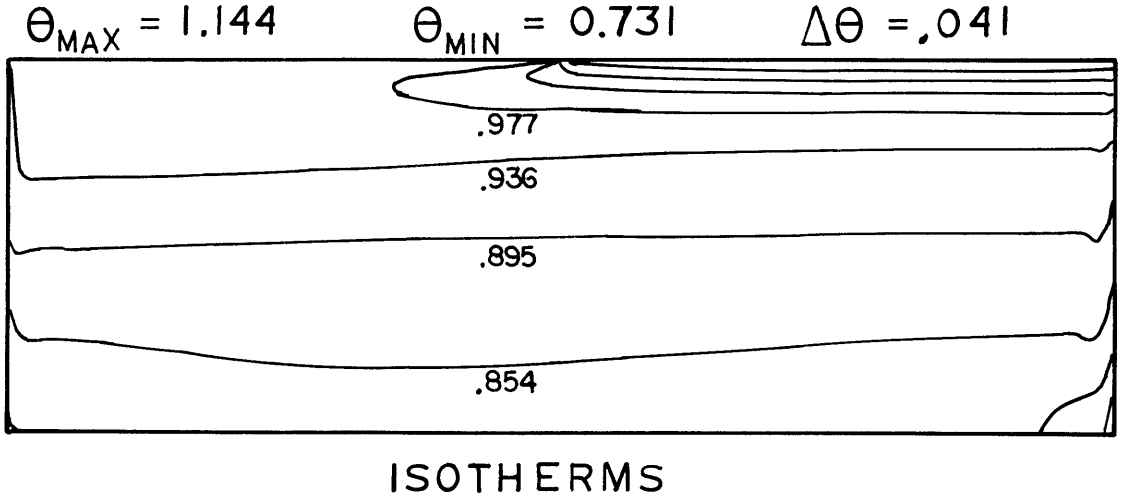

Figure 11. Computed Isotherms and Streamlines for Longitudinal Section--Centerline (Run 119)

dog house wall, thus creating the large circulation cell. Therefore, the function of this cell is to convect energy from the flame side to the batch, the sink and to the large portion of the molten glass. This larger cell also plays a role in driving the smaller auxiliary cell. Principally driven by bridge wall loss, this smaller cell flows downward along the bridge wall. An energy balance on the longitudinal section gives some indication of the validity of the numerical solution. The heat losses on the various boundaries are shown in Table IX. As would be expected, the major heat losses occurred on the batch zone and along the bridge wall. In conjunction with the side walls heat losses, it should be noted that its inclusion as uniformly distributed point heat sinks serves to displace the maximum stream function point to the region farther from the dog house wall than without Φ. (In previous cases, the maximum stream function points are always shown near the left hand upper corner (17)). Since the side wall heat losses are affected by the convective flow, it suggests that some portion of the longitudinal flow changes its direction to transverse flow.

3. Numerical Run for the Transverse Sections

Because of the symmetry of the problem, it is necessary to carry out the calculation for the half plane only. Therefore, aspect ratio is specified as $A_T/2=1.5$. The boundary conditions are:

TABLE IX. Dimensionless Energy Balance for Longitudinal Section

Heat Loss to Batch	= - 3.4264
Heat Loss to Doghouse Wall	= - 0.3207
Heat Loss to Bridge Wall	= - 1.1188
Heat Loss to Bottom	= - 0.2224
Heat Loss to Side Walls (as heat sinks)	= - 0.5656
TOTAL ENERGY OUTPUT	= - 5.6539
TOTAL HEAT INPUT (From Flame Side)	5.6562
% CLOSURE ON TOTAL BALANCE	= 0.04%

$$z = 0 \qquad 0 \leq x \leq 1 \qquad \psi = \frac{\partial \psi}{\partial x} = \frac{\partial \psi}{\partial z} = 0 \qquad -\frac{\partial \theta'}{\partial z} = Nu_s(\theta' - \theta_A) \tag{22}$$

$$z = 1.5 \qquad 0 \leq x \leq 1 \qquad \psi = \frac{\partial \psi}{\partial x} = \frac{\partial^2 \psi}{\partial z^2} = 0 \qquad \frac{\partial \theta'}{\partial z} = 0 \tag{23}$$

$0 \leq z \leq 1.5 \qquad x = 0$

(1) Batch cover $\qquad \psi = \frac{\partial \psi}{\partial x} = \frac{\partial \psi}{\partial z} = 0 \qquad \theta' = \theta_s$ (24)

(2) Flame side $\qquad \psi = \frac{\partial^2 \psi}{\partial x^2} = \frac{\partial \psi}{\partial z} = 0 \qquad -\frac{\partial \theta'}{\partial x} = q_F^*$ (25)

$$0 \leq z \leq 1.5 \qquad x = 1 \qquad \psi = \frac{\partial \psi}{\partial x} = \frac{\partial \psi}{\partial z} = 0 \qquad -\frac{\partial \theta'}{\partial x} = Nu_B(\theta' - \theta_A) \tag{26}$$

It should be noted that the solutions show symmetry about the centerline z=1.5. To obtain a complete transverse section solution, we can take advantage of this symmetry property, such that

$$\begin{aligned} \psi(x,z) &= -\psi(x, A_T - z) \\ \theta'(x,z) &= \theta'(x, A_T - z) \end{aligned} \qquad 0 \leq z \leq 1.5 \tag{27}$$

is preserved by the equations.

Source-sink functions are assumed constant along the z-direction and may be obtained by using a central difference formula which is second-order correct.

$$SI_L(i,k) = \frac{-2}{\Delta x_{i-1}}\left[\left(\frac{(\theta_{i-1,j^*} - \theta_{i,j^*})}{\Delta x_{i-1} + \Delta x_{i-2}}\right) + \left(\frac{\theta_{i+1,j^*} - \theta_{i,j^*}}{\Delta x_{i-1} + \Delta x_i}\right)\right] - \Phi \qquad (28)$$

for $3 \leq I \leq M$.

where the superscript stars in the indices refer to the specified longitudinal section. If the zone in question is adjacent to a boundary, that is i=2, M+1, the correct formulation may be obtained by letting $\Delta x_o = \Delta x_{MP1} = 0$. Along the boundary, all source-sink functions are set to zero.

For several positions in longitudinal sections, source-sink function values are calculated from equation (28), which are listed in Table X. It shows that most of the heat source regions exist under the batch cover and that the largest sources are located near the terminus of the batch cover. Clearly, the largest energy transfer to a third dimension also occurs between the top surface source/sink pair, even though this relatively large source is confined within a narrow depth (x≈0.04). It is interesting to note that the other heat source regions appeared to correspond to the small circulation cell and the appending small cell (at the lower left corner) of the longitudinal section flow. Furthermore, total strength of source-sink functions for any transverse section is nearly constant under the flame side, but increases along the y direction under the batch cover.

TABLE X. Source-Sink Functions for Transverse Section

Run Number	No. 11	No. 31	No. 6	No. 3	No. 15
y =	0.054	1.111	2.940	4.590	5.904
Region	Batch	Batch	Batch	Flame	Flame
x_i					
1	0	0	0	0	0
2	0.2509	1.2129	420.54	-7.8776	-14.3776
3	0.5851	3.5846	36.011	-12.3046	-10.7081
4	0.5155	3.0624	-3.9676	-9.5817	- 7.7614
5	0.3289	1.0076	-3.6935	-4.8722	- 5.2606
6	0.3032	0.4300	-1.0293	-1.9207	- 1.7710
7	0.6187	0.8358	-0.0763	-0.5285	- 0.9519
8	1.7438	0.6734	-0.0362	-0.0793	- 0.1096
9	0.3592	-0.4219	-0.2143	-0.0075	+ 0.1671
10	-1.1176	-0.5513	-0.2177	0.0642	0.2999
11	-1.1868	-0.3529	-0.1721	0.0617	0.5622
12	0.1879	-0.1761	-0.1578	-0.1452	1.0570
13	0.3543	-0.0823	-0.1537	-0.3748	1.4264
14	-0.1541	-0.0993	-0.1234	-0.4156	- 0.4215
15	-1.5704	-0.0741	-0.0730	-0.2829	- 5.0604
16	-2.3759	-0.0396	-0.0284	-0.1202	- 5.8778
17	0	0	0	0	0
Total Strength* of source-sink function	0.07053	0.3220	8.6774	-1.8483	- 1.8512

(* = $\sum_i$ SI(I,K)*Δx(I)

Results and Discussion

Table XI summarizes the computed output data for the five different transverse sections, for which source-sink functions are defined in Table X. Computed isotherms and streamline plots are shown in Figure 12, 13, 14, 15 and 16. In these runs, 15x16 grid system is defined by stretched coordinate systems was used. For the acceptability of results, fairly stringent criteria set forth for the test case were used.

Table XI and five figures show that, by and large, the flow patterns in transverse section can be identified with two distinct zones: zone with two circulations and with one circulation zone. And the two zones are almost exactly corresponding to the batch cover zone and flame size zone, respectively. Several authors (4, 18) have already studied the flow patterns under the flame side zone. The qualitative descriptions are apparently in agreement with those authors and can be read in their papers. The flow patterns under the batch cover will be explained in the subsequent section.

As would be expected, the circulation rate in the transverse section is quite small compared with that for the longitudinal section. Under the flame side zone, circulation rates are almost constant for various sections and the magnitude is approximately 1/40 of that of longitudinal section (ψ^*=1.15 vs 42.13). It is quite evident then, that the heat supplied by the flame side is mainly transported into

TABLE XI. Summary of Dimensionless Results for Transverse Sections

Run Number	No. 11	No. 31	No. 6	No. 3	No. 15	Remarks
y =	.054	1.111	2.940	4.590	5.904	
Region	Batch	Batch	Batch	Flame	Flame	
θ_{max}	.9434	.9576	1.0403	1.1450	1.1430	
θ_{min}	.8160	.8378	.8398	.8327	.7872	
ψ_{max}	6.09	4.57	1.56	1.14	1.15	Primary Cell
	1.05	1.59	.82	-	-	Secondary Cell
U_{Max}	59.56	50.51	15.25	14.20	15.88	Vertical Velocity
W_{max}	-38.56	-41.53	10.92	-9.97	-10.58	Transverse Velocity
TR_{max}	.01	.01	.02	.02	.02	Temp. Residual
Energy Balance						
Q_{Batch}	-.1150	-.8639	-25.926	.0	.0	
$Q_{S.W.*}$	-.1137	-.1347	-.1363	-.1369	-.1363	*for one side wall only
Q_{Bottom}	-.1096	-.1138	-.1141	-.1128	-.1043	
Q_{SI}	.4944	1.2489	26.315	-5.2621	-5.2708	
Q_{Source}	.0	.0	.0	5.6562	5.6562	
Q_{Input}	.4944	1.2489	26.315	5.6562	5.6562	
Q_{Output}	-.4929	-1.2472	-26.313	-5.6487	-5.6477	
% Closure on Total Input	.03	.14	.01	.13	.15	

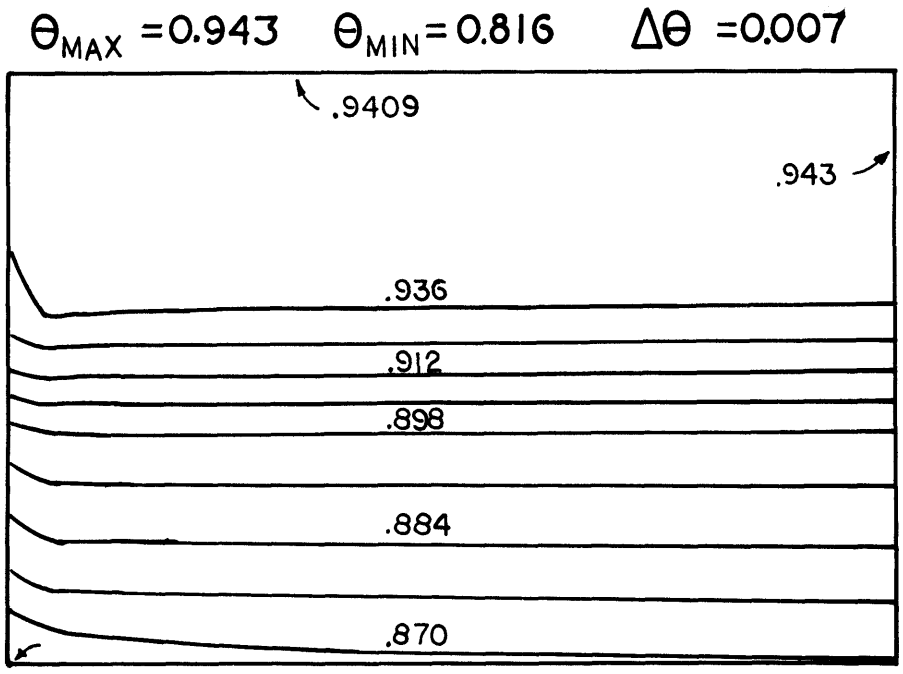

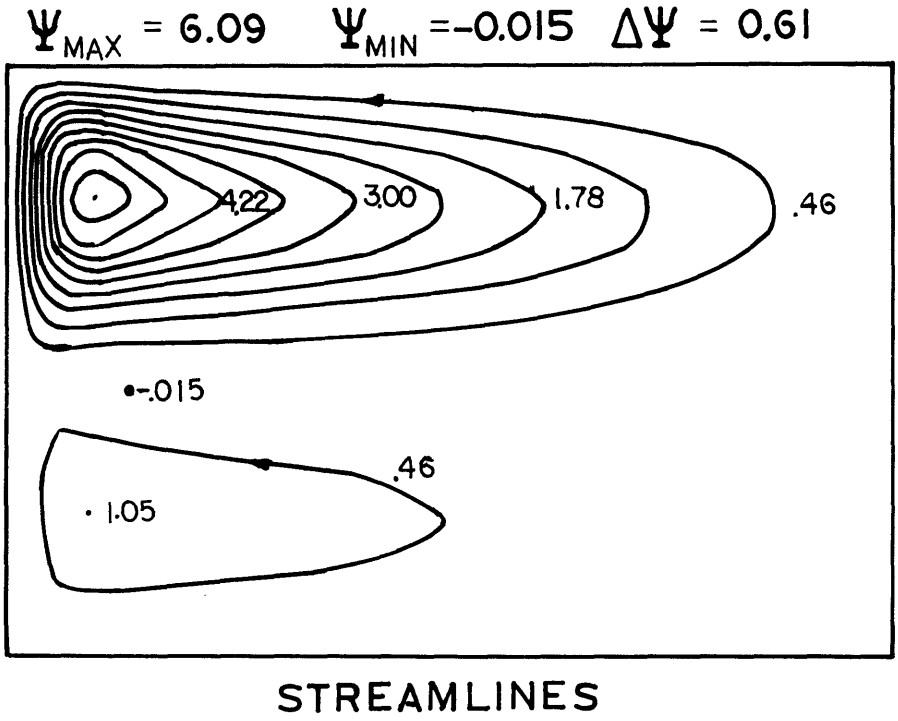

Figure 12. Computed Isotherms and Streamlines for Transverse Section -- y = 0.054 (BATCH)(Run 11)

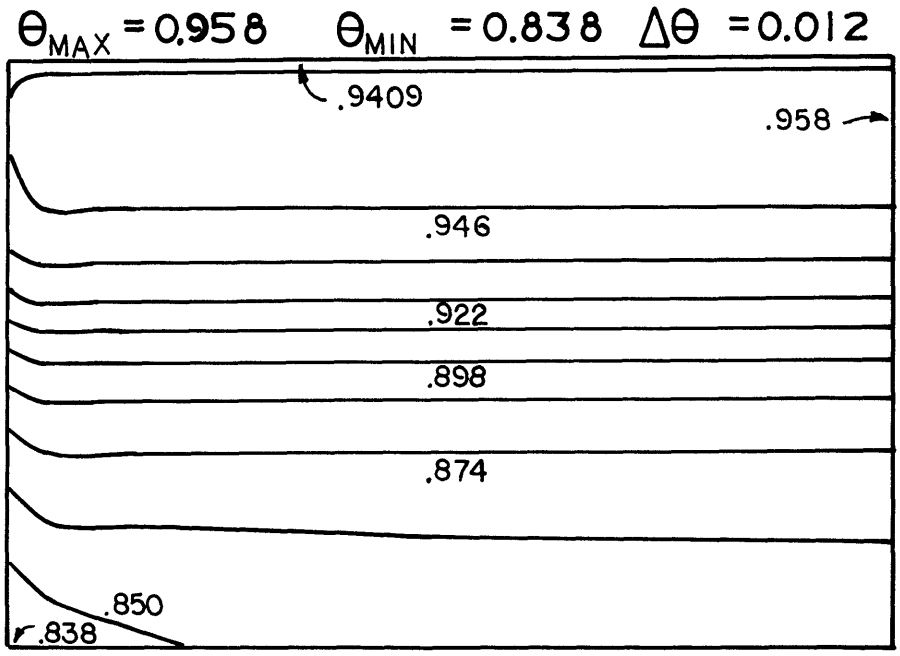

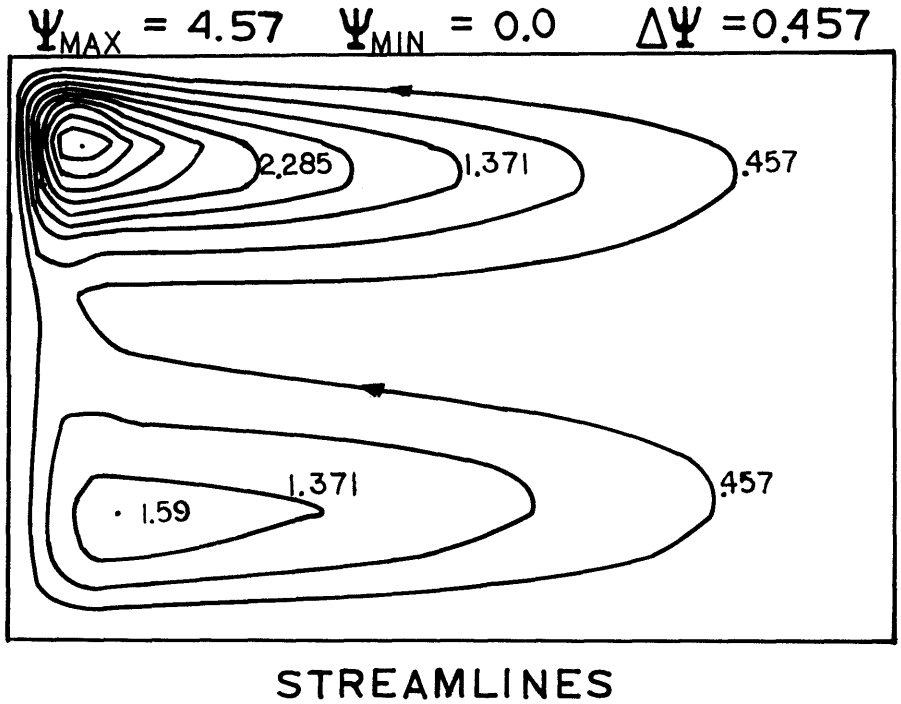

Figure 13. Computed Isotherms and Streamlines for Transverse Section -- y = 1.111 (BATCH) (Run 31)

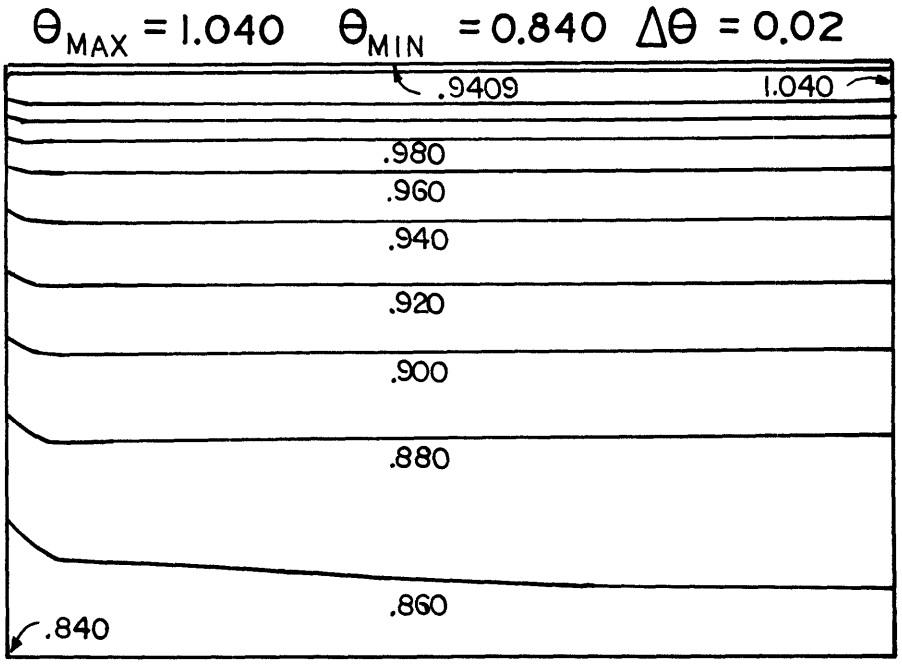

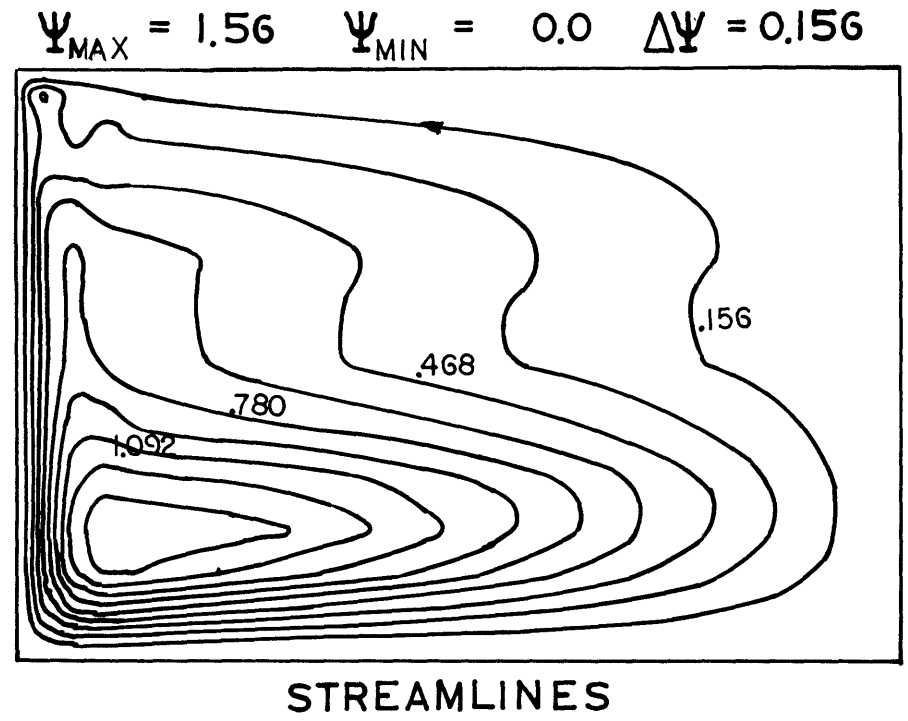

Figure 14. Computed Isotherms and Streamlines for Transverse Section -- y = 2.940 (BATCH)(Run 6)

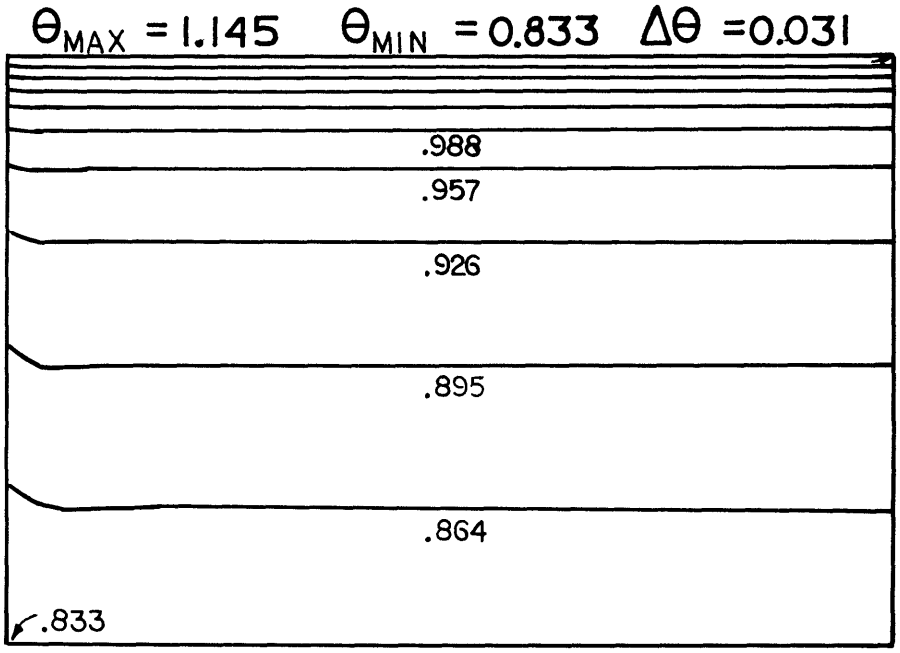

ISOTHERMS

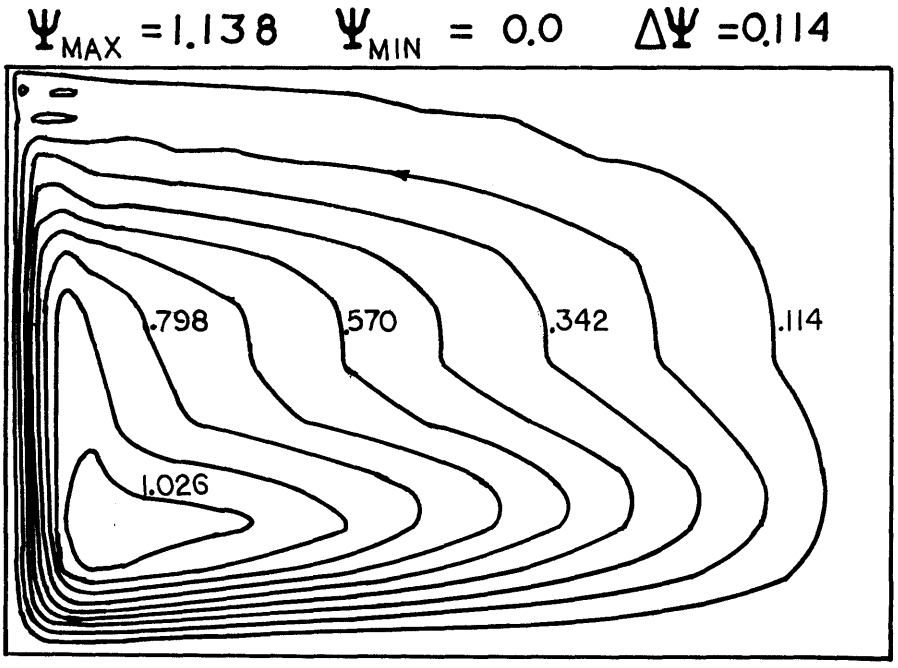

STREAMLINES

Figure 15. Computed Isotherms and Streamlines for Transverse Section -- y = 4.590 (FLAME)(Run 3)

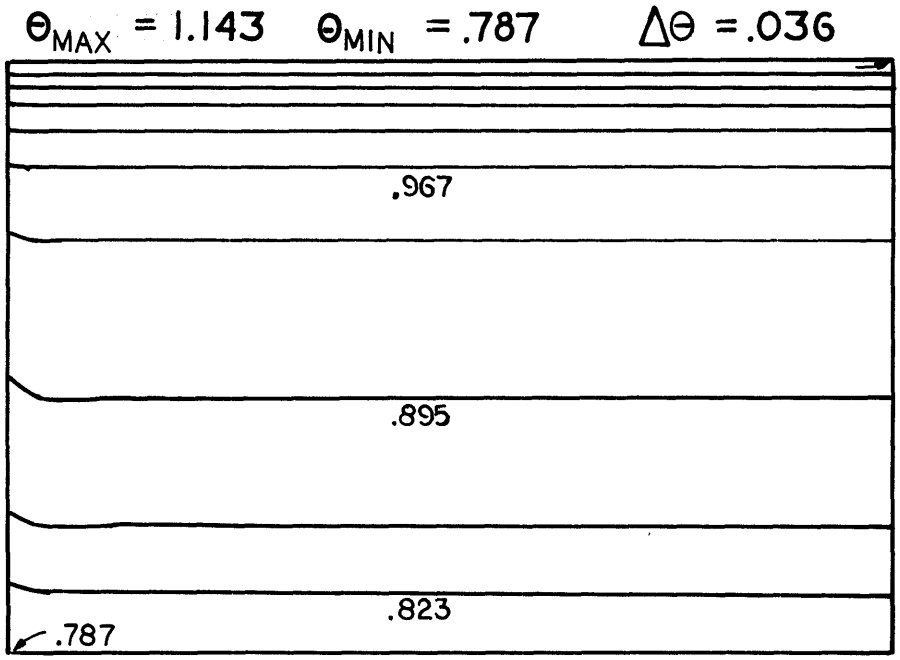

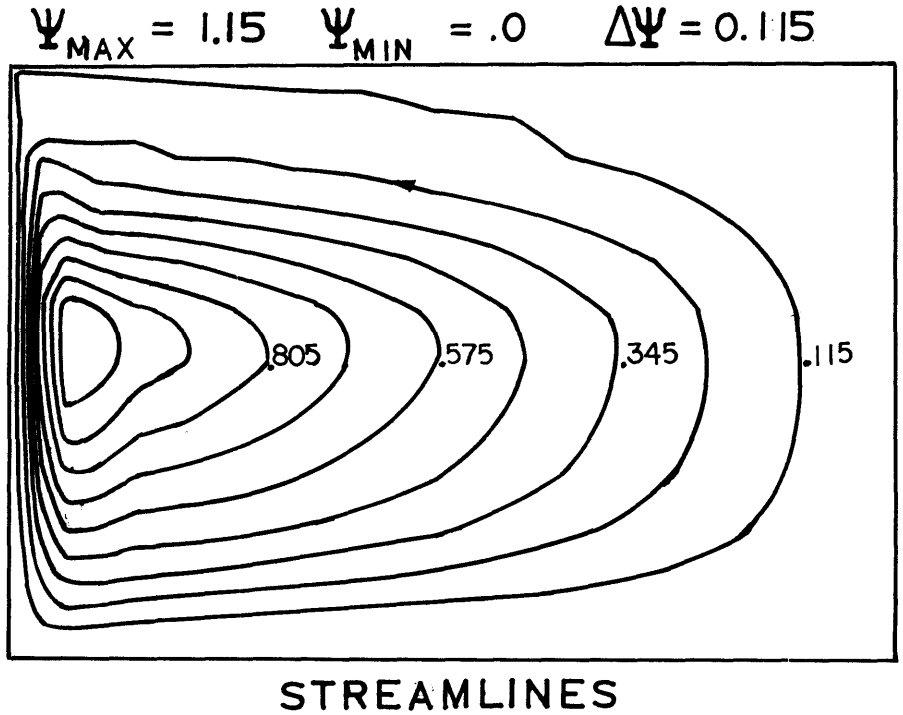

Figure 16. Computed Isotherms and Streamlines for Transverse Section -- y = 5.904 (FLAME)(Run 15)

the batch cover zone through the longitudinal convection flow. In other words, longitudinal flows under the flame side are little perturbed due to the transverse section flow. The streamline map (Figure 15) shows this feature. Here the maximum point of stream function is pushed down the side wall. In Figure 16, which corresponds to weaker longitudinal cell near the bridge wall, the maximum stream function point is displaced upward.

When the longitudinal convective flow enters into the batch cover zone and proceeds toward the doghouse wall, the circulation rate in transverse section increases progressively and finally reaches its maximum value (ψ=6.1) near the dog house wall (Figure 12). The ratio of the transverse to the maximum longitudinal flow ranges from 1/6 to 1/10. Here the flow patterns are quite different from those of the flame side. Two circulation cells are formed, the upper cell being stronger than the lower one, (Figure 12 and 13) , and they are in same rotation sense. Thus a stagnant region is introduced in the mid-height to minimize the shear stress between them. It is interesting to note that this shear layer between each cell coincides with regions of relatively large vertical temperature gradient, or conduction (Figure 12 and 13).

This kind of shear layer zone was confirmed from photographs and visual observations by Elder (6). Even though he investigated convection flow in vertical slot,

the flow regime under the batch cover has many resemblences to his problem. Thus two inner circulation cells correspond to his secondary flow. The most intriguing feature of his study was the formation of tertiary flow. As the shear layer becomes thicker, he observed that a new flow was formed which formed a circulation with closed streamlines between the secondary flow cells. The corresponding cell is also shown in Figure 12, where minimum stream function value is negative, though quite small (due to the large interval between streamlines used in stream function plot, this cell does not show itself in this figure). While the primary and secondary flows have the same sense of circulation (counterclockwise in the figure) the tertiary flow is in the opposite sense (clockwise in the figure).

Also indicated in Table XI are the maximum and minimum temperatures and the computed heat balances for the entire transverse sections. Here again, the distinction between the batch cover region and the flame side region is observed from their different heat sources. Particularly, under the batch cover region, internal sources (positive source-sink functions) are the only heat sources and all boundaries are losing heat to the ambient and batch. Even though the melt is thermally stratified almost everywhere, hotter areas of fluid exist within the melt displaced from the top batch surface, as shown in Figure 12, 13 and 14. This seemingly unstable distribution of temperature (in view of two dimensional

problem) plays an important role on the formation of two circulation cells, as will be explained in subsequent section. The vertical temperature profiles at the symmetry line in Figure 17 show this feature clearly.

The increase in transverse circulation rate toward the dog house wall is clearly related to the distribution of source-sink functions within the transverse section. It is to be noted that in Table X, the position where maximum source exists becomes progressively deeper as one approaches the dog house wall, even though the total strength of source-sink functions as well as the magnitudes of their maxima decreases considerably along this direction. This fact suggests that the magnitude of the circulation rate has nothing to do with the magnitude of maximum source and the total strength of source-sink functions, but with the distance between the maximum source and the primary heat sink (i.e. batch cover). Physically, an increase in this distance makes effective Rayleigh number larger, which in turn results to increase circulation rate. Furthermore, the position of source below the sink (contrary to the flame side cases) is in favor of the motion of fluid elements acting with buoyancy force.

4. Formation of Two Necessary Circulation Cells under the Batch Cover

It is instructive to present a physical explanation of the formation of two circulation cells.

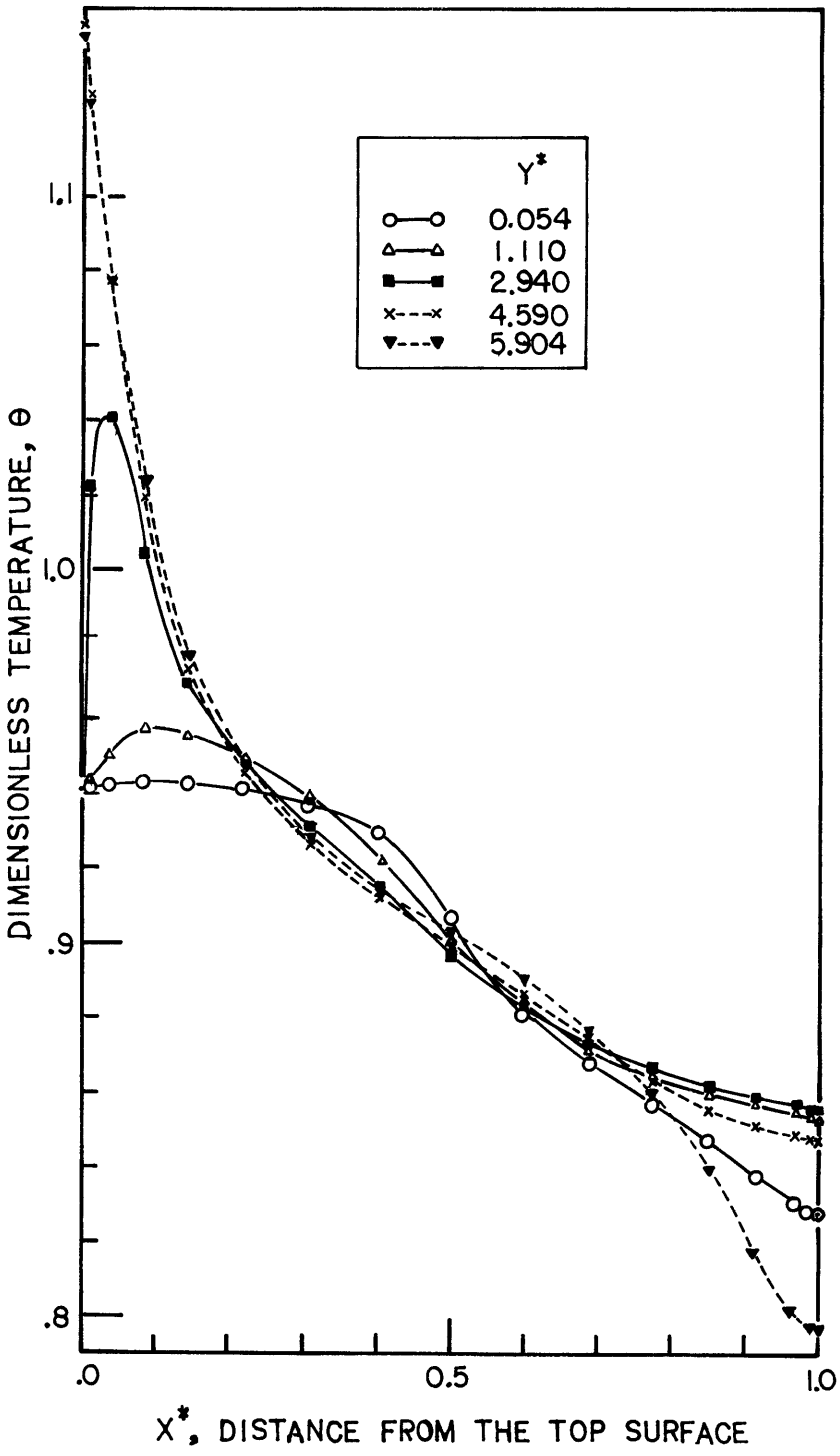

Figure 17. Vertical Temperature Profiles at Centerline (Transverse Section Results)

Consider a fluid particle in the boundary layer on the batch cover and suppose that it is losing heat by conduction. This loss of heat must be reflected by movement of the particle to a colder part of the fluid. If there is stable vertical temperature gradient (i.e. $\partial\theta/\partial x<0$), this will generally mean movement toward the bottom. But, with the horizontal gradient as well as an adverse vertical temperature gradient (see Figure 17), horizontal movement ($w<o$) will carry the particle to a colder zone, i.e. side wall, and so it should move toward the side wall.

When the fluid particle turns around the left upper corner, two possibilities occur. A particle adjacent to the side wall will continue to lose heat by conduction, thus moving along the sidewall to the bottom. The situation is quite different when the particle is closer to the hotter part of the fluid. There is nothing to balance the inward diffusion of heat except the horizontal convection toward the core region, which is the only possible warmer region that particular particle can find. This leads to the formation of upper circulation cell.

A fluid particle located away from both the side wall and the bottom surface but in the lower half section experiences a very slight gain of heat due to vertical conduction of heat. At first, it is likely to move upward. However, the horizontal temperature gradient along the side wall immediately prevents this purely upward movement and induces a horizontal convection flow toward the side wall. When this

particle becomes in proximity to the side wall, heat loss to this wall forces it downwards. Thus lower circulation cell is formed.

The presence of hotter part of fluid within the narrow top layer causes to make the upper circulation cell stronger than the lower one. The interaction of two circulation cells of same rotation sense needs some smooth transition change so as to minimize the otherwise shear friction between them. Therefore, in the mid-height fluids forms weak shear layer or nearly stagnation point.

The horizontal velocity profiles are plotted against the distance from the top surface in Figure 18. These profiles are representative of the velocities at or near the maximum stream function points (z=1.465). Under the flame side, boundary layers are formed only near the bottom and down the side wall. However, under the batch cover, flow reversals occur in the upper half and lower half sections and the flow is much stronger in the upper half than the lower half. In the mid-height, the horizontal velocity components are very small, as would be expected from above explanation.

5. Revised Results for Longitudinal Section

Only the centerline longitudinal section was investigated to obtain various transverse section flows. In order to construct a three-dimensional picture of the flow patterns, it is necessary to study how the flow patterns in transverse sections can influence on the various longitudinal section

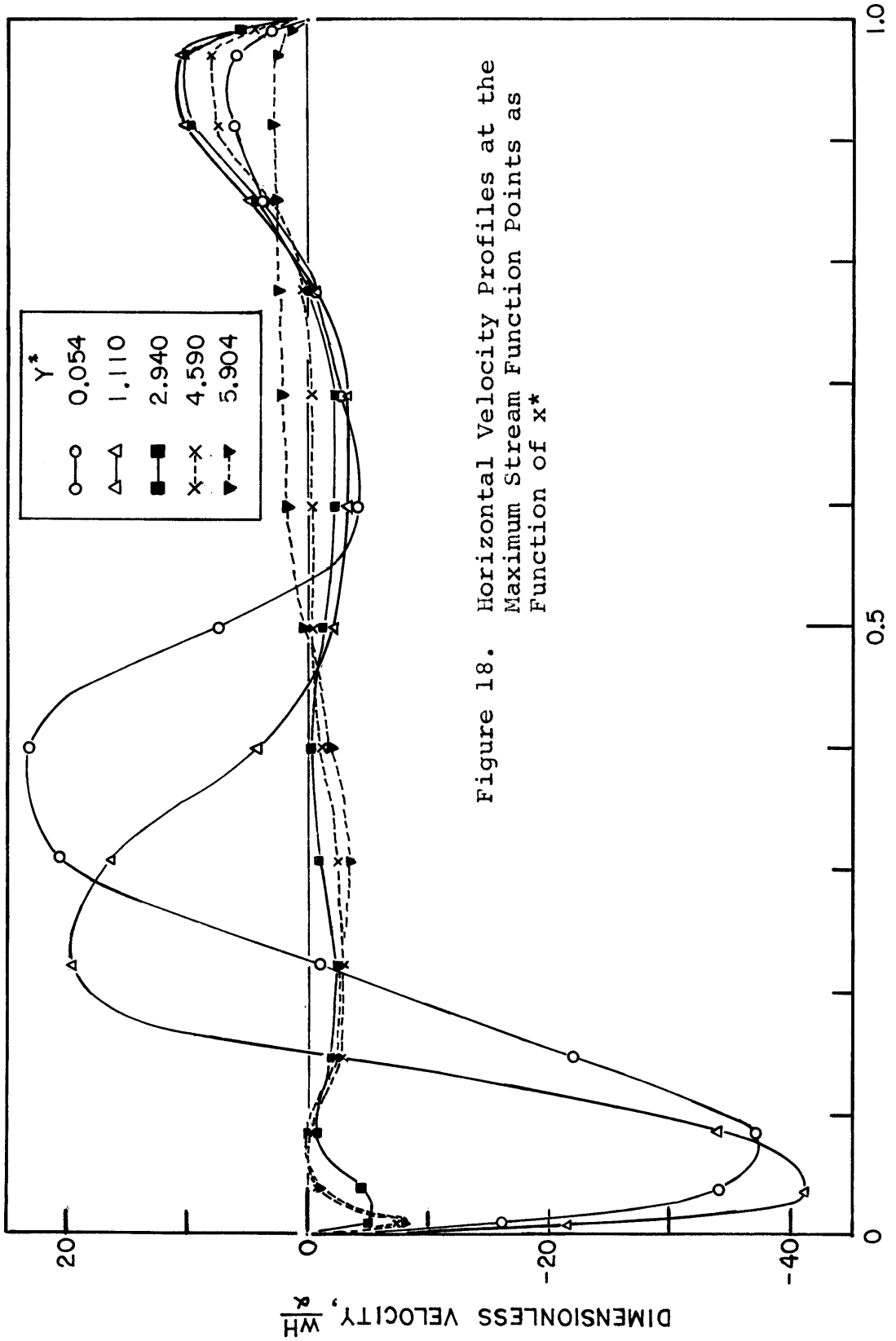

Figure 18. Horizontal Velocity Profiles at the Maximum Stream Function Points as Function of x*

flows. This requires solutions of equation (21) in Chapter III, where source-sink functions are defined.

$$SI_L = - \left. \frac{\partial^2 \theta'}{\partial x^2} \right|_T - SI_T \qquad (29)$$

In order to calculate the second derivative term, the glass furnace is split of five basic regions, which are characterized by the thermal behavior of the enclosure: boundary layer zone near the bridge wall, the stratified core zone under the flame side, the transition zone between the batch cover and the flame side, the stratified zone under the batch cover and finally, the boundary layer zone near the dog house wall. The representative flow patterns in transverse sections which correspond to the above five basic zones have been investigated in the previous section 3. From the pertinent temperature fields, five source-sink functions, SI_L, were calculated and assigned to represent each of the basic zones (i.e. T = 36~28, 27~22, 21~15, 14~7 and 6~1). Two longitudinal sections are chosen to perform numerical calculations. The sections chosen are located at z=1.5 (centerline) and z=0.3751 (near the side wall).

The computed isotherms and streamlines are shown in Figure 19 and 20. Compared to the original longitudinal flow pattern (Figure 11), they show no significant change in both temperature and stream function field. While the maximum temperatures are slightly lowered, the maximum value of stream functions show a small increase. The results

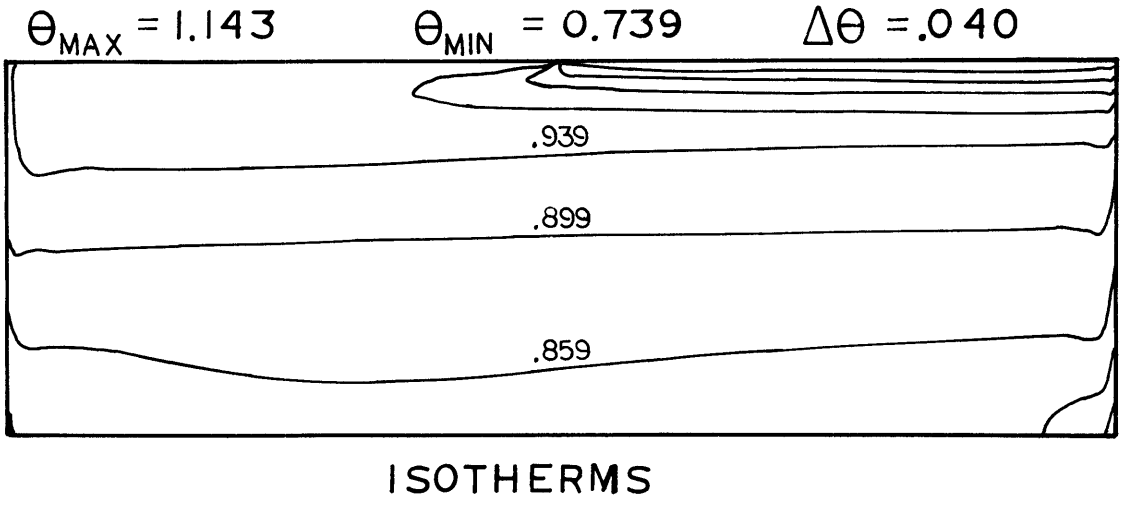

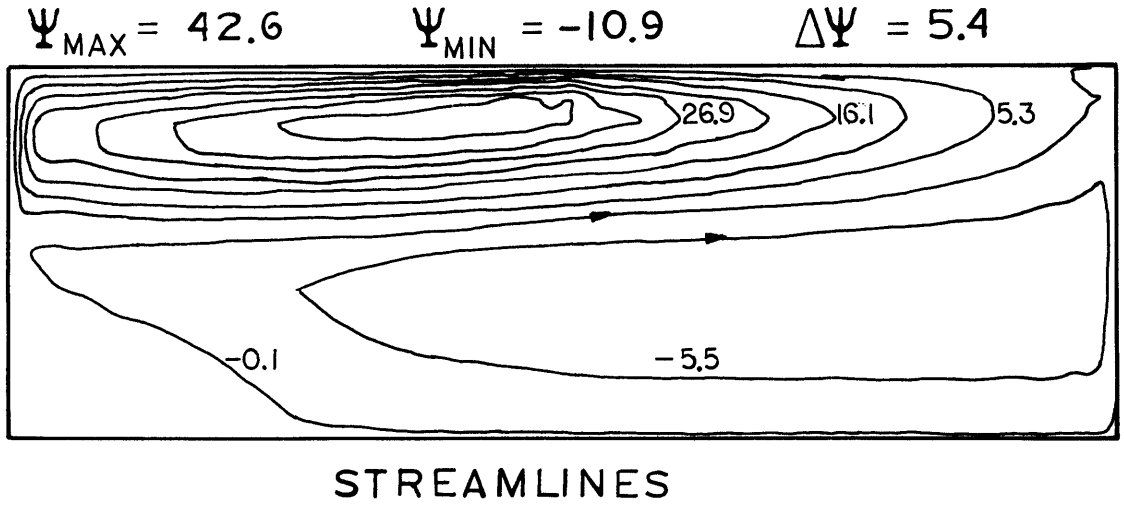

Figure 19. Computed Isotherms and Streamlines for Longitudinal Section - z = 1.5 (Centerline) (Run 120)

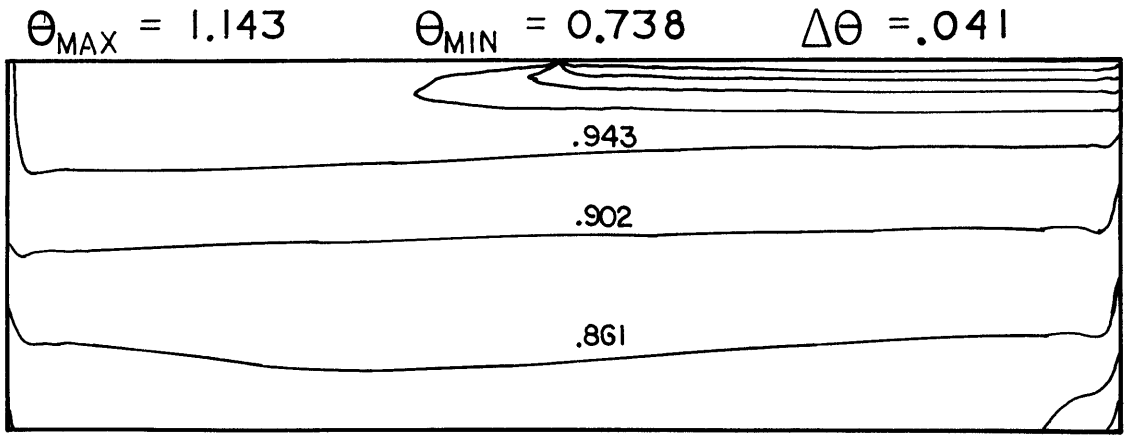

ISOTHERMS

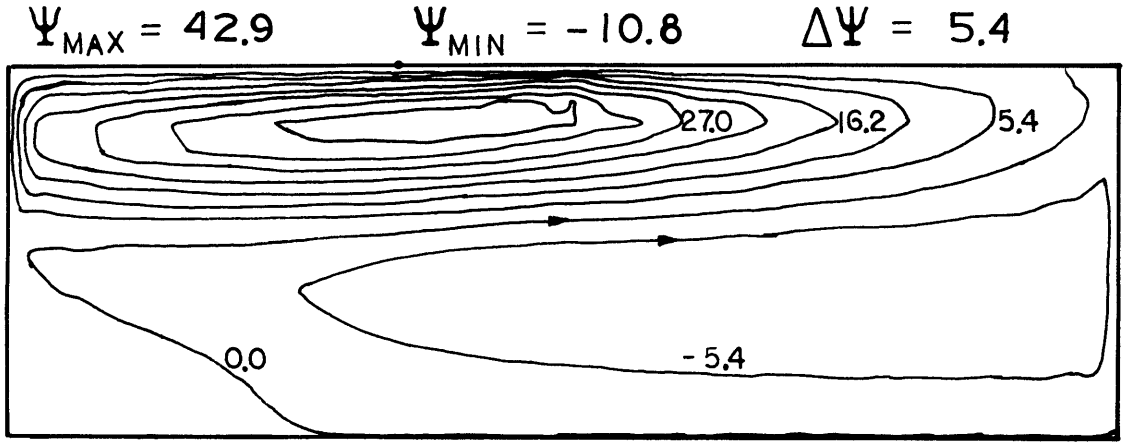

STREAMLINES

Figure 20. Computed Isotherms and Streamlines for Longitudinal Section - z = 0.3751 (Run 121)

may be expected from examination of source sink functions employed, because all the boundary conditions are strictly identical for three cases. For the original longitudinal section, uniform source sink (ϕ=0.09427) was assumed. For the latter two cases, source-sink functions were assigned different values in each grid zone, but they did not deviate very much from the original Φ values. That is, the term $-\partial^2\theta'/\partial x^2$ is largely compensated by the term $\partial^2\theta/\partial x^2$, resulting in the value of SI_L which is almost equal to Φ values.

Comparison of two different longitudinal streamline plots (Figure 19 and 20) shows that maximum values of stream functions are slightly increased as one approaches from centerline to the side wall (ψ= 42.6 to 42.95). This cannot be fully explained. It may be caused by the crude zoning assignments.

Finally a picture of flow and temperature profiles emerges from the careful combination of the transverse and longitudinal results. In view of the above longitudinal section results, there seems no further calculations are necessary. The complete solutions may be further refined when one insists on thorough calculations for every grid point.

V. CONCLUDING REMARKS

An approximation method has been devised which describes the three dimensional flow patterns in glass furnace as a composite of two orthogonal two-dimensional solutions. In order to suppress the extraneous motions due to non-uniform spacing in grid, stretched coordinate system was used.

With reference to the derivation of source-sink function, the intrinsic limitation and approximation demands that the results should have to be checked by more rigorous solution or by experimental data.

The extension of this method to the case of variable thermal conductivity does not pose any difficulties. For the more realistic simulation of glass furnace however, material throughput should be incorporated in the proposed method. In this case, stream function values should be assigned along the boundary surfaces.

With the grid system 15x34x16 employed in this study, the required computer time for the complete results may be estimated about 25 min CPU time in IBM 370/Model 165. The computing cost is not at all expensive, compared to the other programs (for example, see reference (2)). Furthermore, it can provide detailed descriptions on the transverse section flow patterns.

APPENDIX A. Description of CONRAD Program

The dimensionless equations describing the transport of energy and momentum by source-sink approximation method are summarized in Table II. Inspection of these equations shows that the common forms to be solved are:

The Energy Equation:

$$\frac{\partial \theta}{\partial t} + \frac{\partial (u\theta)}{\partial x} + \frac{\partial (v\theta)}{\partial y} = \frac{\partial^2 \theta}{\partial x^2} + \frac{\partial^2 \theta}{\partial y^2} + S(x,y) \qquad (1)$$

The Biharmonic Equation:

$$\frac{1}{N_{Pr}} \frac{\partial \nabla^2 \psi}{\partial t} + \frac{\partial}{\partial x} (u\nabla^2 \psi) + \frac{\partial}{\partial y}(v\nabla^2 \psi)$$

$$= - N_{Ra} \frac{\partial T}{\partial y} + \frac{\partial}{\partial x}(\nu \frac{\partial \nabla^2 \psi}{\partial x}) + \frac{\partial}{\partial y}(\nu \frac{\partial \nabla^2 \psi}{\partial y}) \qquad (2)$$

where

$$u = \frac{\partial \psi}{\partial y} \quad \text{and} \quad v = - \frac{\partial \psi}{\partial x}$$

which satisfies the continuity equation. The CONRAD 8 Program is designed to solve these equations. Basically, the finite difference scheme used to solve these equations is that described for CONRAD 7 in L. A. Clomburg's thesis (4). The principal differences between CONRAD 7 and CONRAD 8 need some mention on the material contained in this appendix.

First, the terms necessary for the source-sink model of the three-dimensional tank have been incorporated. To specify the source-sink function as input fields, logical variable LOGIC takes the value of 3. Also the type of source-sink function should be specified by the new logical value LOGSS. For typical problems to be solved under this method, LOGSS assumes the value of 2 with UOLD = 0.0. With the sufficiently reliable data on the x component of the velocities, designation of u velocities can perform to calculate the term $u\frac{\partial \delta \theta}{\partial x}$ (for this purpose, LOGSS=3). As mentioned already, this term is explicitly incorporated in the program. Thus it is to be noted that the calculated results of this term always assume the value one step behind the current time step. Next, the computation efficiency is improved by the compaction of the algorithm. This has been achieved through the calculation of all the distance coefficients once in VGRID and the elimination of the use of the function operators DXSQ, DYSQ, and the solution routines, DIAG5 and THOMAS present in CONRAD 7. All these operations have been incorporated directly into STREAM and THICK. The result of this change shows a twofold decrease in the computer time needed per iteration.

The alternative method for computing the iteration parameter applied to the energy equation is another feature of the CONRAD 8. This parameter is not only computed independently from the OPTIM, but also provides optimum value at each node point to insure more rapid convergence of energy

equation. For the coupled equations, CCONST=π should be designated.

Lastly, a simple plotting routine has been incorporated into the program to obtain a line printer plot of the temperature and stream function fields thereby enabling one to visualize the results more readily. Also the input of the initial conditions and boundary conditions have been generalized and simplified by changing the ICON routine.

Due to the above revisions in CONRAD 8, the logic flow is somewhat different from CONRAD 7, and is outlined in Figure 21. The MAIN program controls the operation of the entire algorithm. Various input data are read in and various derived constants are computed by the Main Program. Then the VGRID is called, in which the variable grid size is read in, and the distance coefficients for the derivative operators are calculated. The subroutine ICON is followed and the boundary and initial conditions and source-sink functions are read in or generated. The initial transfer factors, viscosity, thermal conductivity and velocity are then computed by calling SPEED. SUBROUTINE OPTIM is then called to compute the iteration parameters BETAF, BETAV and ALPHA. All the data which have been read in and other derived parameters are then printed out by the subroutine TITLE.

The principal computation loop is then entered. After checking various control parameters for transient output, time and iteration number, the time-step and iteration numbers

FIGURE 21. CONRAD8 PROGRAM FLOW CHART

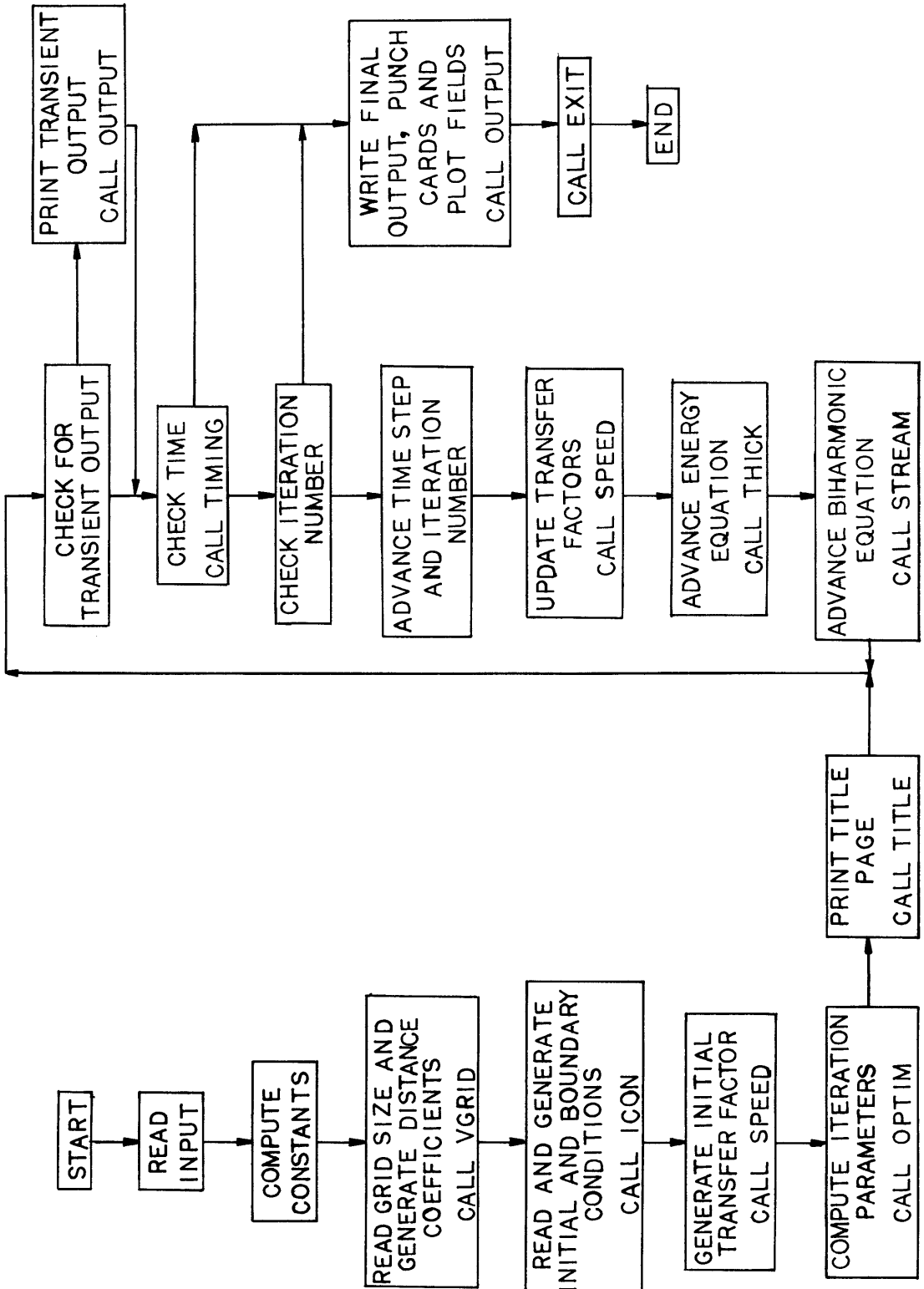

are advanced and the updated transfer factors are computed by calling SPEED. The energy equation is then advanced by calling THICK and STREAM is then called to advance the biharmonic equation. This results in new values of temperature and stream function, and the entire process is repeated. The program is terminated either when the maximum number of iterations has been exceeded, or when the job time has been exceeded. Then the final output is printed and plotted and punched on cards for use in subsequent runs.

A complete listing of the CONRAD 8 program will be found in the thesis to be published by N.W.E. Curlet.

APPENDIX B. Scaling Problem of Natural Convection in Transverse Section of Glass Tank

Consider the following geometry and boundary conditions

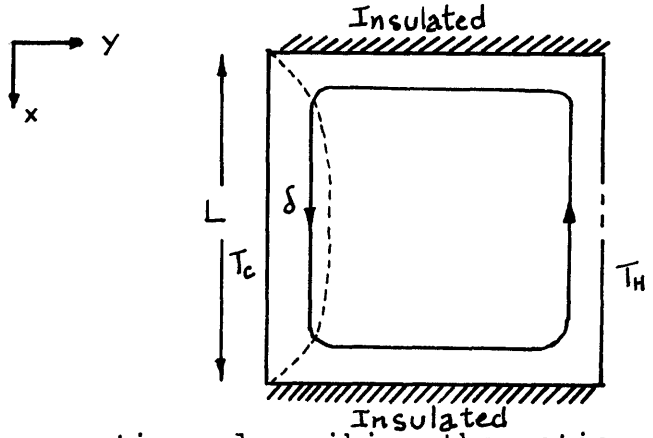

The equations describing the motion may be written:

Energy:

$$\frac{\partial(uT)}{\partial x} + \frac{\partial(vT)}{\partial y} = \alpha \frac{\partial^2 T}{\partial x^2} + \alpha \frac{\partial^2 T}{\partial y^2} \tag{1}$$

Momentum:

$$\frac{\partial(uu)}{\partial x} + \frac{\partial(uv)}{\partial y} = g\beta\Delta T - \frac{1}{\rho_o}\frac{\partial p}{\partial x} + \frac{\partial}{\partial x}(\nu\frac{\partial u}{\partial x}) + \frac{\partial}{\partial y}(\nu\frac{\partial u}{\partial y}) \tag{2}$$

$$\frac{\partial(uv)}{\partial x} + \frac{\partial(vv)}{\partial y} = - \frac{1}{\rho_o}\frac{\partial p}{\partial y} + \frac{\partial}{\partial x}(\nu\frac{\partial v}{\partial x}) + \frac{\partial}{\partial y}(\nu\frac{\partial v}{\partial y}) \tag{3}$$

Continuity:

$$\frac{\partial u}{\partial x} + \frac{\partial v}{\partial y} = 0 \tag{4}$$

The stream functions may be defined to satisfy the continuity equation.

$$u = \frac{\partial \psi}{\partial y} \qquad \text{and} \qquad v = -\frac{\partial \psi}{\partial x} \tag{5}$$

The momentum equation may be combined to eliminate the pressure terms with the introduction of vorticity ω

$$\frac{\partial (u\omega)}{\partial x} + \frac{\partial (v\omega)}{\partial y} = g\beta \frac{\partial T}{\partial y} + \nu \left[\frac{\partial^2 \omega}{\partial x^2} + \frac{\partial^2 \omega}{\partial y^2} \right] \tag{6}$$

where

$$\omega = \nabla \times \vec{v} = -\nabla^2 \psi \ . \tag{7}$$

Now we want to choose scaling parameters for normalizing these equations for the following reasons:

(1) to scale the dependent variables to computationally feasible ranges,

(2) to determine the dimensionless groups and the relationship between these groups which describe the problem,

(3) to gain physical insight of the effect of these groups on the system operation.

Obviously our choice of scaling parameters has to be based on the region which is most important because there are different modes of energy and momentum transfer in different regions. In this case, we note that there are both hydrodynamic and thermal boundary layers along the vertical walls. With large Prandtl numbers, the inertia forces are indeed small compared to the viscous forces. While the heat transfer into the fluid can only be by conduction, heat transfer from the hot wall to the cold wall is mainly by convection. It suggests that we

should equate the conductive and convective transfer to be consistent with the preponderance of viscous forces in fluid.

Suppose the thickness of the boundary layers on the vertical walls is of order δ. From the boundary layer nature of the flow at the vertical walls, δ is much smaller than the vertical dimension L. A balance between convection and conduction (in eq. 1) requires that

$$\frac{u_s T}{L} = \frac{\alpha T}{\delta 2} \tag{8}$$

A balance between buoyancy and viscous forces in (2) also produces

$$g\beta\Delta T = \frac{\nu u_s}{\delta 2} \quad \text{where } \Delta T = T_H - T_C \tag{9}$$

Combining (8) and (9) we have

$$\delta = \frac{R_a^{-1/4}}{L} \quad \text{where } R_a = \frac{g\beta\Delta T L^3}{\nu\alpha} \tag{10}$$

Then the order of magnitude ψ of the stream function can be deduced from the equation (5) with equation (10)

$$\psi = u_s \delta = \nu \frac{R_a^{1/4}}{Pr} = \alpha Ra^{1/4} \tag{11}$$

Now, let us examine the core where the horizontal and vertical space scales are the same, L. A balance between the convective and conductive terms in (1), we get

$$\frac{u}{L} \sim \frac{\alpha}{L^2} \tag{12}$$

$$\text{i.e. } u_s \sim \frac{\alpha}{L} \tag{13}$$

Thus

$$\psi_s \sim \alpha \quad \text{and} \quad \omega_s \sim \frac{\alpha}{L^2} \tag{14}$$

This implies the equations to be solved should be

$$\frac{DT^*}{Dt^*} = \nabla^2 T^* \tag{15}$$

$$\frac{1}{Pr}\frac{D\omega^*}{Dt^*} = Ra\,\frac{\partial T^*}{\partial y^*} + \nabla^2\omega^* \ , \tag{16}$$

which is the equation system that CONRAD 8 program can solve. This is in contrast to the results obtained from equating viscous forces with inertia forces:

$$\frac{DT^*}{Dt} = \frac{1}{Pr}\nabla^2 T^* \tag{17}$$

$$\frac{D\omega^*}{Dt} = Gr\,\frac{\partial T^*}{\partial y^*} + \nabla^2\omega^* \qquad \text{where} \quad Gr = \frac{\beta g L^3 \Delta T}{\nu^2} \tag{18}$$

This system of equations was employed by Chen and Goodsen (2) to solve three dimensional model of an electrical furnace. The inspection of equation (17) shows that it is clearly in error at the boundary layer region where the conductive fluxes are the only form of energy transport (though in an electrical furnace, convective fluxes are not quite so important).

NOMENCLATURE

Symbol	
A	Aspect ratio
B	Extent of batch coverage
C	Fractional batch coverage
c_p	Specific heat
$\delta u, \delta v, \delta w$	Perturbation velocity components
E	Constant in variable viscosity law
$g, \vec{g}$	Gravitational constant or vector
H	Height of furnace
K	Total a sorption coefficient
k, ke, krad	True, effective and radiative thermal conductivity
L	Length of furnace
$N_{Nu}=\frac{UH}{k_{eo}}$	Dimensionless heat transfer coefficient (Nusselt number)
$N_{Ra}=\frac{\beta g H^3 T_R}{\alpha_{eo}\nu_o}$	Rayleigh number
$N_{vis}=E/T_R$	Viscosity number
n	Index of refraction
P	Pressure
Q, q	Total heat flux and local heat flux density
SI	Source-sink function denoting internal heat generation rate
T	Temperature
t	Time
U	Overall heat transfer coefficient

U,V,W	True cartesian velocity component
u,v,w	Three dimensional cartesian velocity component
$\vec{v}$	Velocity vector
W	Width of enclosure
x,y,z	Cartesian position coordinates

Greek

α_e	Effective thermal diffusivity
β	Volumetric coefficient of thermal expansion
Θ,θ	Dimensionless temperature
λ	Wavelength
μ	Viscosity
ν	Kinematic viscosity
ρ	Density
σ	Stefan-Boltzmann Constant
Φ	Internal energy generation rate (representing side wall loss)
ψ	Stream function
ω	Vorticity

Superscripts

*	Denotes dimensionless quantity
'	Denotes transverse section temperature or velocity fields
"	Denotes longitudinal section temperature or velocity fields

Subscripts

A	Denotes ambient condition
B,BW,DW,SW	Denotes bottom, bridge wall, dog house wall, and side wall, respectively
F	Refers to flame side
L	Refers to longitudinal section
R	Denotes reference quantity
T	Denotes transverse section
o	Denotes physical property evaluated at temperature T_o

Special Numerical Nomenclature

M,N,K	Number of grid zones in the x,y,z direction
u,v,w	Dimensionless velocities
x,y,z	Dimensionless coordinates
Δx, Δy, Δz	Zone height, length and width
i,j,k(I,J,K)	Subscript referring to the numerical coordinate of a quantity
ξ,η	Ordinate in stretched coordinate system

LITERATURE CITATIONS

1. Aziz, K., and Hellums, J. D., "Numerical Solution of the Three-dimensional Equations of Motion for Laminar Natural Convection", Phys. Fluids, 10(2) 314-324 (1967).
2. Chen, T.-S., and Goodsen, R. E., "Computation of Three-dimensional Temperature and Convective Flow Profiles for an Electric Glass Furnace", Glass Tech., 13(6) 161-167 (1972).
3. Chorin, A. J., "Numerical Solution of the Navier-Stokes Equations", Math. Comp., 22, 745-762 (1968).
4. Clomburg, L. A., "Mathematical and Experimental Modeling of the Circulation Patterns in Glass Melts", Ph.D. Thesis, Chem. Eng. Dept., M.I.T. (1971).
5. Crowder, H. J., and Dalton, C., "Errors in the Use of Nonuniform Mesh Systems", J. Comput. Phys. 7, 32-45 (1971).
6. Elder, J. W., "Laminar Free Convection in a Vertical Slot", J. Fluid Mech., 23 (11), 77 (1965).
7. Gill, A. E., "The Boundary-Layer Regime for Convection in a Rectangular Cavity", J. Fluid Mech., 26 (3), 515-536 (1966).
8. Gunther, R., "Glass-Melting Tank Furnaces", Soc. of Glass Tech., England (1958).
9. Hottel, H. C., and Sarofim, A. F., "Radiative Transfer", pp 331-337, McGraw-Hill, New York (1967).

10. Knudsen, J. G., and Katz, D. L., "Fluid Dynamics and Heat Transfer", pp 101, McGraw-Hill, New York (1958).

11. Moore, D. R., and Weiss, N. O., "Two-dimensional Rayleigh-Bénard Convection", J. Fluid Mech., 58 (2), 289-312 (1973).

12. Noble, J. J., "The Effect of Radiative Transfer on Natural Convection in Enclosures - A Numerical Investigation", Ph. D. Thesis, Chem. Eng. Dept., M.I.T. (1968).

13. Noble, J. J., Clomburg, L. A., Sarofim, A. F., and Hottel, H. C., "Mathematical and Experimental Modeling of Circulation Patterns in Glass Melts", Trans. ASME, J. Heat Transfer 94 c(2), 149-154 (1972).

14. vonPeschke, J., "Computation of Convection Currents in Glass Melts" (Berechnung von Konvektionsströmungen in Glassmelzwannen), Glastechn. Ber., 38(7), 276-281,(1965).

15. DeRivas, E. K., "On the Use of Nonuniform Grids in Finite-Difference Equations", 10, 202-210 (1972).

16. Schneck, P., and Veronis, G., "Computation of Some Recent Experimental and Numerical Results in Bénard Convection", Phys. Fluids., 10(5), 927-930 (1967).

17. Spiegel, E. A., and Veronis, G., "On the Bousinesq Approximation for a Compressible Fluid", J. Astrophys., 131(12), 442 (1960).

18. Trier, W., "Relationship between Temperature Field and Flow Field by Free Convection in Glass Melts", (Zusammanhang zwischen Temperaturfeld und strömungsfeld bei Freier Konvektion in Glasschmelzen), Glastechn.Ber., 38(7), 282 (1965).

19. Williams, G. P., "Numerical Integration of the Three-dimensional Navier-Stokes Equations for Incompressible Flow", Fluid Mech. 37(4) 727-750 (1969).

20. Wright, S., and Rawson, H., "Calculation of Natural Convection in a Rectangular Cell Containing Glass with Specified Temperatures on the Boundaries", Glass Tech. 14(2), 42-48 (1973).